PHYSICAL REVIEW D VOLUME 33, NUMBER 3 1 FEBRUARY 1986

Spin splittings in heavy quarkonia

James Pantaleone* and S.-H. Henry Tye
Newman Laboratory of Nuclear Studies, Cornell University, Ithaca, New York 14853

Yee Jack Ng
Institute of Field Physics, Department of Physics and Astronomy, University of North Carolina, Chapel Hill, North Carolina 27514
(Received 29 August 1985)

The spin-dependent potentials in the formalism of Eichten and Feinberg and Gromes are generalized. Consistency of the observed spin splittings in the J/ψ and Υ systems with QCD imposes stringent constraints on the type of nonperturbative spin-dependent forces allowed.

I. INTRODUCTION

Quarkonium physics has been extensively studied in the past decade.[1-6] The effective spin-independent potential $E(r)$ between a heavy quark and a heavy antiquark is essentially determined by a combination of theory and phenomenology. In the region $0.1 \leq r \leq 1$ fm, which is probed by the J/ψ and the Υ spectroscopies, a flavor-independent potential has emerged which appears to be determined by experimental data. At shorter distances perturbative quantum chromodynamics (QCD) is applicable, and it predicts the form of the potential $E(r)$ at $r < 0.1$ fm. This prediction depends only[6-8] on the QCD scale parameter $\Lambda_{\overline{\rm MS}}$ which is 0.1 GeV $\leq \Lambda_{\overline{\rm MS}} \leq 0.5$ GeV, where $\overline{\rm MS}$ denotes the modified minimal-subtraction scheme. It turns out that the available $(Q\bar{Q})$ data do not probe short enough distances to unambiguously extract the precise value of $\Lambda_{\overline{\rm MS}}$. At large distances, i.e., $r > 1$ fm, the potential is expected to rise linearly. Here, the effects of open channels also become important. These effects have been studied in detail.[3,9]

In contrast, the understanding of the spin-dependent forces in the quarkonium systems is much less satisfactory. The literature on spin-dependent forces in quarkonium is extensive.[10-18] A popular approach has been to start from the Bethe-Salpeter equation and an instantaneous kernel with some suitably chosen Lorentz structure, and to deduce the corresponding Breit-Fermi Hamiltonian. An assumption on the long-range force must be made in order to confront the experimental data. Unfortunately, there is little theoretical understanding of the nature of this long-range spin-dependent force. The situation can be illustrated by two recent detailed treatments which use somewhat different kernels. The approach by Moxhay and Rosner[13] (MR) has a kernel with a long-range potential which is a mixture of scalar, vector, and tensor forces. The approach by McClary and Byers[14] (MB) has a purely scalar long-range potential. The resulting spin-dependent forces are quite different.

In our opinion, the approaches mentioned above and other similar approaches are conscientious attempts in understanding the spin-dependent forces; however, in general, they suffer from some of the following problems.

(1) The form of the long-range spin-dependent forces is arbitrary; in principle, the long-range spin-dependent forces are completely determined by the dynamics of QCD. However, at this moment such a determination turns out to be too difficult. As a result, the choice of the long-range spin-dependent forces are based on phenomenological arguments that cannot be substantiated on theoretical grounds.

(2) The value of the running QCD coupling constant α_S used in spin-dependent forces is taken from the spin-independent potential or elsewhere. In principle, different physical processes will have different tree-level coupling constants; the common parameter is $\Lambda_{\overline{\rm MS}}$, not α_S. In fact, α_S in the hyperfine splitting and α_S in the fine structure, even in the same quarkonium system, need not have the same value.

(3) The QCD radiative corrections can be important but are not included in the many analyses of spin-dependent forces. They contribute to the spin-dependent forces in a form different from the tree-level terms.

The inclusion of QCD radiative corrections to the spin-dependent forces has been carried out by two groups: the hyperfine structure by Buchmüller, Ng, and Tye[15] (BNT) and the fine and hyperfine structures by Gupta, Radford, and Repko[16,18] (GRR). In this paper, we shall reexamine the spin-dependent forces from the viewpoint of perturbative QCD. By comparing the $(c\bar{c})$ and the $(b\bar{b})$ bound systems data with the perturbative QCD expressions for the hyperfine and fine structures, we extract eight determinations of the $\Lambda_{\overline{\rm MS}}$ parameter. Consistency requires a common value for $\Lambda_{\overline{\rm MS}}$, if perturbative QCD alone is sufficient to explain the data. This consistency constraint provides us with valuable insights to the presence (or absence) of other effects in the spin-dependent forces. Our approach is feasible because of the existence of the new data on the fine structures in the Υ system. Better data are expected in the future. We believe our approach is meaningful because the effects of light quarks, or the coupled channel effects, can be ignored in the analysis of the spin-dependent potentials. Let us give a brief sketch of our approach as well as our intuitive viewpoint on the issues.

First, let us adopt the formalism of Eichten and Fein-

berg[10] and Gromes[12] (EFG). They start from QCD and obtain the form of the spin-dependent potential V_{SD} via an expansion in inverse powers of the quark mass. This allows the inclusion of long-range and/or nonperturbative effects. However, we find that the EFG formalism is inadequate: for the unequal-mass case ($m_1 \neq m_2$, for quark mass m_1 and antiquark mass m_2) additional terms must be included in V_{SD}; for both the $m_1 = m_2$ and the $m_1 \neq m_2$ cases, some of the terms in V_{SD} are actually flavor dependent. The spin-dependent potentials must be generalized to include the quark-mass dependence, i.e., $V_i(r) \to V_i(m_1, m_2, r)$ in the EFG formalism. The new formalism will be referred to as the generalized EFG formalism. We include the one-loop QCD radiative correction contribution in V_{SD}.

The inclusion of the QCD radiative correction in V_{SD} serves three purposes.

(1) Formalism. As mentioned above the one-loop QCD effect allows us to explicitly show that the $1/m$ expansion for the V_{SD} is not valid. There are terms of the form $\ln(m_1/m_2)$ and $\ln[(m_1 m_2)^{1/2} r]$ which invalidate the original EFG formalism. Such terms also suggest the appropriate generalizations.

(2) Phenomenology. Irrespective of any other corrections, the QCD radiative corrections definitely contribute to the spin-dependent potential V_{SD}. The question is whether or not such corrections are important; and if they are important, whether the inclusion of QCD radiative corrections alone is sufficient to explain the data.

(3) Theoretical consistency. The inclusion of one-loop QCD effects allows us to replace the strong-coupling parameter α_S by the QCD scale parameter $\Lambda_{\overline{MS}}$. Consistency requires that the same value of $\Lambda_{\overline{MS}}$ be used in the quarkonium potential, the hyperfine and the fine structures.

For simplicity, let us assume for the moment that, to a good approximation, V_{SD} is completely given by the perturbative QCD results (i.e., no long-range, nonperturbative spin-dependent force). From the J/ψ and Υ systems the data on the spin-spin, the spin-orbit, and the tensor terms together allow us to make eight independent determinations of the $\Lambda_{\overline{MS}}$ parameter (as more data become available, more independent determinations can be made). Consistency demands that, within errors, a common value of $\Lambda_{\overline{MS}}$ should be obtained if our assumption is correct. This consistency requirement allows us to obtain insight on the long-range spin-orbit term and other nonperturbative terms. If a common value of $\Lambda_{\overline{MS}}$ cannot be obtained, it means other effects must be important, such as nonperturbative instanton effects, the gluon condensate effects, the relativistic corrections and/or the light-quark effects (beyond their contributions to the vacuum polarization), as well as a long-range spin-dependent force. On the other hand, if a common value of $\Lambda_{\overline{MS}}$ is obtained, we can then use it to predict values of the hyperfine and the fine-structure splittings with better precision than the present data have.

Our results are summarized in Fig. 1, where $\Lambda_{\overline{MS}}$ is obtained by comparing the perturbative QCD expressions with the data. We observe that, with the inclusion of the QCD one-loop renormalization-group improved contribution, and with a choice of $\Lambda_{\overline{MS}} = 0.30$ GeV, the hyperfine and the fine-structure splitting can be accounted for. (See *Note added,* where $\Lambda_{\overline{MS}} \simeq 0.40$ GeV is obtained.) No long-range (nonperturbative) spin-dependent force or any other corrections are necessary for the Υ system (see *Note added).* For the charmonium system, some additional effects, such as relativistic corrections, are needed. In general, relativistic corrections in the Υ spectroscopy are expected to be substantially smaller than that in the ψ/J spectroscopy. As we shall see, the choice of no long-range spin-orbit is in good agreement with the Υ data. Improvement in the data will certainly sharpen the comparison.

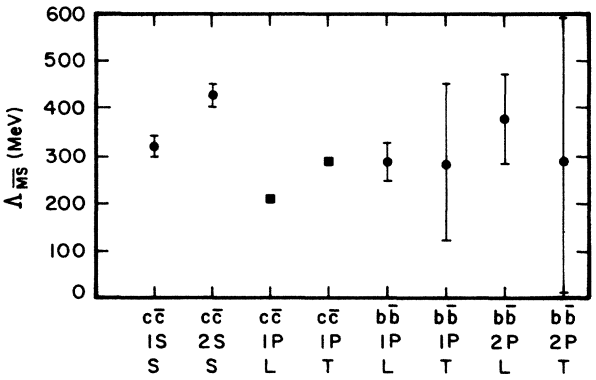

FIG. 1. The value of the $\Lambda_{\overline{MS}}$ parameter obtained by comparing the perturbative QCD expressions (with $N_F = 3$) for the hyperfine (S) term, the spin-orbit (L) term, and the tensor (T) term with the experimental values for the $\psi - \eta_c$ $(1S), \psi' - \eta_c'(2S)$, the χ_c, χ_b, and the χ_b' splittings. The errors are experimental only. For details, see text.

In Sec. II we present the one-loop QCD radiative correction to the spin-dependent potential V_{SD}. This is essentially a summary of the results in Refs. 15, 16, 18, and 21–23. In Sec. III the spin-dependent potential V_{SD} is cast into the generalized EFG formalism. In Sec. IV we summarize the data on the hyperfine and the fine-structure splittings in the J/ψ and the Υ spectroscopies. In Sec. V we discuss our approach to extracting the QCD scale parameter $\Lambda_{\overline{MS}}$ from the data. A rather detailed discussion on the theoretical uncertainties is also included. In Sec. VI we discuss possible forms for the long-range spin effects and their implications on the value of $\Lambda_{\overline{MS}}$. In Sec. VII we briefly discuss the earlier approaches to the spin-dependent forces. In Sec. VIII some predictions on the t-quarkonium system are discussed. Section IX contains the conclusion and some remarks. Our *Note added* gives an update of the analysis. Some details are relegated to appendixes. Appendix A contains a brief review of the two prescriptions used extensively in the text, namely, the Grunberg[35] and the Brodsky-Lepage-Mackenzie[36] (BLM) prescriptions. Appendix B gives the numerical values for the quarkonium potential used in the text. Appendix C presents a sample calculation of $\Lambda_{\overline{MS}}$ from the experimental data.

II. PERTURBATIVE CALCULATION OF THE POTENTIAL

A. Equal mass

In this section we present the results of the fourth-order quark-antiquark interactions in perturbative QCD. The Feynman diagrams (Fig. 2) and their individual contribution to the effective Hamiltonian ΔH are shown below. The results for the individual diagrams refer to the Feynman gauge. (Of course, the whole set of graphs is gauge invariant.) We use dimensional regularization[19] for ultraviolet divergences, and a small gluon mass λ to regularize infrared divergences. For spin-independent interactions we have kept terms to

$$O\left[\frac{\alpha_S}{m^2}\right],\ O\left[\frac{{\alpha_S}^2}{m\,|\mathbf{Q}|}\right]$$

(α_S is the unrenormalized strong fine-structure constant, $\alpha_S={g_S}^2/4\pi$, $\mathbf{Q}$ is the momentum transfer, and m is the mass of the quark or antiquark). We have treated the spin-dependent terms more accurately to

$$O\left[\frac{\alpha_S\,|\mathbf{Q}|}{m^3}\right],\ O\left[\frac{{\alpha_S}^2}{m^2}\right].$$

Except for the diagram containing the three-gluon vertex, all the diagrams also appear in QED and their results are known. Let us introduce the following notations for the hyperfine, the spin-orbit, and the tensor couplings:

$$S=\boldsymbol{\sigma}_1\cdot\boldsymbol{\sigma}_2\,, \tag{2.1}$$

$$L=-i\frac{(\boldsymbol{\sigma}_1+\boldsymbol{\sigma}_2)}{2}\cdot\frac{\mathbf{Q}\times\mathbf{p}}{\mathbf{Q}^2}\,, \tag{2.2}$$

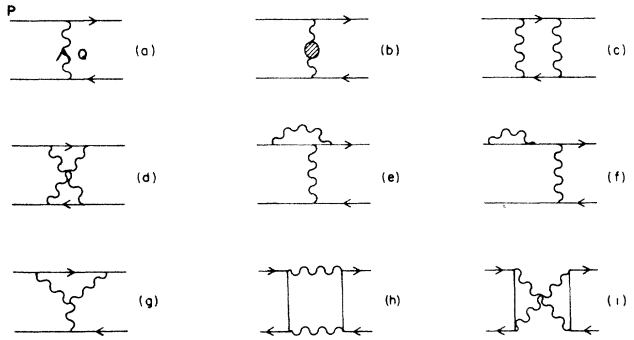

FIG. 2. The Feynman diagrams contributing to the quark-antiquark potential in order α_S and order ${\alpha_S}^2$.

$$T=\frac{(\boldsymbol{\sigma}_1\cdot\boldsymbol{\sigma}_2)\mathbf{Q}^2-3(\boldsymbol{\sigma}_1\cdot\mathbf{Q})(\boldsymbol{\sigma}_2\cdot\mathbf{Q})}{\mathbf{Q}^2}\,, \tag{2.3}$$

where $\boldsymbol{\sigma}$ and $\mathbf{p}$, respectively, denote the spin ($\mathbf{S}=\boldsymbol{\sigma}/2$) and momentum (in the center-of-mass frame) of the quark and the antiquark. Referring to Fig. 2, diagram (a) gives the second-order contributions

$$\Delta H(a)=\frac{\pi\alpha_S}{m^2}C_F\left[-\frac{4m^2}{\mathbf{Q}^2}+2-\frac{4\mathbf{p}^2}{\mathbf{Q}^2}+\frac{2}{3}S+\frac{1}{3}T+6L\right]. \tag{2.4}$$

Figure 2(b) contributes

$$\Delta H(b)=\Pi(Q)\Delta H(a)\,, \tag{2.5}$$

where[20]

$$\Pi(Q)=\frac{\alpha_S}{4\pi}\left[\left(-\tfrac{5}{3}C_A+\tfrac{4}{3}T_FN_f\right)\left[-\frac{2}{\epsilon}+\gamma_E-\ln4\pi+\ln\frac{\mathbf{Q}^2}{\mu^2}\right]+\tfrac{31}{9}C_A-\tfrac{20}{9}T_FN_f\right] \tag{2.6}$$

and $\epsilon=4-D$ for D space-time dimensions, μ is the renormalization scale, $\gamma_E=0.5772\ldots$, the Euler constant, and N_f the number of massless quark flavors. T_F, C_F, and C_A are gauge group factors. T_F is the normalization of generators which we take to be $\frac{1}{2}$. C_F is the quadratic Casimir for the fermion representation and C_A is the quadratic Casimir for the adjoint representation. For SU(N), $C_F=(N^2-1)/2N$, and $C_A=N$. In QCD the group factors read $T_F=\frac{1}{2}$, $C_F=\frac{4}{3}$, and $C_A=3$. The one-loop contributions from Figs. 2(c)–2(f) are[21]

$$\Delta H[(c)+(d)+(e)+(f)]=(C_F)^2\left[\frac{\pi^2{\alpha_S}^2}{2m\,|\mathbf{Q}|}-\frac{{\alpha_S}^2}{3m^2}S+\frac{{\alpha_S}^2}{3m^2}(T+12L)\right]+\delta H(\mathrm{d})+\delta H(\mathrm{e})\,, \tag{2.7}$$

where

$$\delta H(\mathrm{d})=-\tfrac{1}{2}C_FC_A\left\{\frac{{\alpha_S}^2}{m^2}\ln\left[\frac{\mathbf{Q}^2}{\lambda^2}\right]\left[-\frac{4m^2}{\mathbf{Q}^2}+\frac{2}{3}S+\frac{1}{3}T+6L\right]+\frac{\pi^2{\alpha_S}^2}{m\,|\mathbf{Q}|}-\frac{{\alpha_S}^2}{3m^2}\left[\left[-1+\tfrac{3}{2}\ln\frac{\mathbf{Q}^2}{m^2}\right]S+T\right]\right\} \tag{2.8}$$

and

$$\delta H(\mathrm{e})=-\frac{\alpha_SC_A}{4\pi}\Delta H(\mathrm{a})\left[\frac{2}{\epsilon}-\gamma_E+\ln4\pi+\ln\frac{\mu^2}{m^2}+2\ln\frac{\lambda^2}{m^2}+4\right]-\frac{{\alpha_S}^2C_FC_A}{6m^2}(2S+T+12L)\,. \tag{2.9}$$

The additional pieces δH(d) and δH(e) are due to the non-Abelian property of the SU(3) color group. For Fig. 2(e), the

upper vertex is given by

$$igT^a\left[\gamma_\lambda F_1(Q^2)+\frac{K_1(Q^2)}{2m}i\sigma_{\lambda\nu}Q^\nu\right],$$

$$K_1(0)=\frac{\alpha_S}{4\pi}(2C_F-C_A), \tag{2.10}$$

$$F_1(Q^2)=\frac{\alpha_S}{8\pi}(2C_F-C_A)\left[\frac{2}{\epsilon}-\gamma_E+\ln 4\pi+\ln\frac{\mu^2}{m^2}+2\ln\frac{\lambda^2}{m^2}+4+O\left[\frac{\mathbf{Q}^2}{m^2}\right]\right].$$

Figure 2(g) contributes

$$\Delta H(\mathrm{g})=\frac{3\alpha_S C_A}{4\pi}\Delta H(\mathrm{a})\left[\frac{2}{\epsilon}-\gamma_E+\ln 4\pi+\ln\frac{\mu^2}{m^2}+\frac{4}{3}+\frac{\pi^2}{6}\frac{|\mathbf{Q}|}{m}\right]+\frac{{\alpha_S}^2 C_F C_A}{6m^2}\left[1+\ln\frac{\mathbf{Q}^2}{m^2}\right](2S+T+12L). \tag{2.11}$$

For Fig. 2(g) the upper vertex is given by

$$igT^a\left[\gamma_\lambda F_2(Q^2)+\frac{K_2(Q^2)}{2m}i\sigma_{\lambda\nu}Q^\nu\right],$$

$$K_2(Q^2)=\frac{\alpha_S}{4\pi}C_A\left[1+\ln\frac{\mathbf{Q}^2}{m^2}+O\left[\frac{\mathbf{Q}^2}{m^2}\right]\right], \tag{2.12}$$

$$F_2(Q^2)=\frac{3\alpha_S C_A}{8\pi}\left[\frac{2}{\epsilon}-\gamma_E+\ln 4\pi+\ln\frac{\mu^2}{m^2}+\frac{4}{3}+\frac{\pi^2}{6}\frac{|\mathbf{Q}|}{m}+O\left[\frac{\mathbf{Q}^2}{m^2}\right]\right].$$

Figures 2(h) and 2(i) also appear in QED.[22] Here their contributions are

$$\Delta H[(\mathrm{h})+(\mathrm{i})]=\frac{{\alpha_S}^2}{m^2}(1-\ln 2)C_F T_F S. \tag{2.13}$$

Summing Eqs. (2.4), (2.5), (2.7), (2.11), and (2.13) we obtain

$$\begin{aligned}\Delta H=&\frac{\pi\alpha_{\overline{\mathrm{MS}}}(\mu)C_F}{m^2}\left[-\frac{4m^2}{\mathbf{Q}^2}+\frac{2}{3}S+\frac{1}{3}T+6L\right]\left[1-\frac{\alpha_S}{2\pi}\ln\frac{\mathbf{Q}^2}{\mu^2}\left(\tfrac{11}{6}C_A-\tfrac{2}{3}T_F N_f\right)+\frac{\alpha_S}{36\pi}(31C_A-20T_F N_f)\right]\\&+\frac{2\pi\alpha_{\overline{\mathrm{MS}}}(\mu)C_F}{m^2}\left[1-\frac{2\mathbf{p}^2}{\mathbf{Q}^2}\right]+\frac{\pi^2\alpha_S^2 C_F}{2m\,|\mathbf{Q}|}(C_F-2C_A)\\&+\frac{{\alpha_{\overline{\mathrm{MS}}}}^2(\mu)C_F}{m^2}\left\{\left[-\tfrac{1}{3}C_F+(1-\ln 2)T_F+\left[-\frac{1}{6}+\frac{7}{12}\ln\frac{\mathbf{Q}^2}{m^2}\right]C_A\right]S+\left[\tfrac{1}{3}C_F+\frac{1}{6}\left[1+\ln\frac{\mathbf{Q}^2}{m^2}\right]C_A\right]T\right.\\&\left.+\left[4C_F+2C_A\ln\frac{\mathbf{Q}^2}{m^2}\right]L\right\},\end{aligned} \tag{2.14}$$

where we have used the modified minimal-subtraction ($\overline{\mathrm{MS}}$) scheme to absorb the pole terms as well as the constant $[\ln(4\pi)-\gamma_E]$ into the definition of the renormalized, scale-dependent coupling constant $\alpha_{\overline{\mathrm{MS}}}(\mu)$, where μ is the renormalization scale. As expected, the infrared divergences have canceled in the sum of Eq. (2.14). The result agrees with that obtained by Gupta and Radford for the equal-mass case.[23] (Of course, the $\sigma_1\cdot\sigma_2$ terms agree with those found[15] by BNT.)

B. Unequal masses

To present the unequal-mass case we must refine our notation of the standard spin-orbit coupling. The symbols for the hyperfine and tensor spin-spin interactions, S and T, remain unchanged from Eqs. (2.1) and (2.3) but the spin-orbit term L now becomes

$$L(1)=-i\frac{(\sigma_1+\sigma_2)}{2}\cdot\frac{\mathbf{Q}\times\mathbf{p}}{\mathbf{Q}^2}, \tag{2.15}$$

$$L(2)=-i\frac{(\sigma_1-\sigma_2)}{2}\cdot\frac{\mathbf{Q}\times\mathbf{p}}{\mathbf{Q}^2}, \tag{2.16}$$

$$L(3)=-i\frac{m_1 m_2}{2}\left[\frac{\sigma_1}{{m_1}^2}+\frac{\sigma_2}{{m_2}^2}\right]\cdot\frac{\mathbf{Q}\times\mathbf{p}}{\mathbf{Q}^2}, \tag{2.17}$$

$$L(4)=-i\frac{m_1m_2}{2}\left[\frac{\sigma_1}{{m_1}^2}-\frac{\sigma_2}{{m_2}^2}\right]\cdot\frac{\mathbf{Q}\times\mathbf{p}}{\mathbf{Q}^2}\ , \tag{2.18}$$

where m_1 is the quark mass and m_2 is the antiquark mass [in the limit of $m_1=m_2$, $L(1)=L(3)=L$]. With this distinction between the spin-orbit terms we can proceed to examine the fourth-order quark-antiquark interaction for unequal-mass quarks. Figure 2(a) gives the second-order contributions

$$\Delta H(a)=\pi\alpha_{\overline{\rm MS}}(\mu)C_F\left[-\frac{4}{\mathbf{Q}^2}+\frac{(m_1+m_2)^2}{2{m_1}^2{m_2}^2}-\frac{4\mathbf{p}^2}{m_1m_2\mathbf{Q}^2}+\frac{2}{3}\frac{1}{m_1m_2}S+\frac{1}{3}\frac{1}{m_1m_2}T+\frac{4}{m_1m_2}L(1)+\frac{2}{m_1m_2}L(3)\right]. \tag{2.19}$$

The term that renormalizes the tree-level expression is the same here as it is in the equal-mass case. The annihilation diagrams, Figs. 2(h) and 2(i), do not contribute to this potential, but there are some qualitatively new interactions. Ignoring contributions that just renormalize the potential, we list below the results from each diagram for the spin-dependent potential.[18] Figures 2(c) plus 2(d) give

$$\Delta H[(c)+(d)]=\frac{{\alpha_S}^2}{2m_1m_2}C_F\left[C_F\left[\frac{4m_1m_2}{{m_1}^2-{m_2}^2}\right]\ln\left[\frac{m_2}{m_1}\right]S+\tfrac{1}{2}C_A\left\{\tfrac{2}{3}T+\left[\ln\frac{\mathbf{Q}^2}{m_1m_2}-\left[\frac{m_1+m_2}{m_1-m_2}\right]\ln\left[\frac{m_2}{m_1}\right]-\frac{8}{3}\right]S\right\}\right]. \tag{2.20}$$

Figure 2(e) gives

$$\Delta H(e)=\frac{{\alpha_S}^2}{2m_1m_2}C_F(C_F-\tfrac{1}{2}C_A)\{\tfrac{2}{3}(2S+T)+4[L(1)+L(3)]\}\ . \tag{2.21}$$

Figure 2(g) gives

$$\Delta H(g)=\frac{{\alpha_S}^2}{2m_1m_2}C_FC_A\left[\left[1+\ln\frac{\mathbf{Q}^2}{m_1m_2}\right][\tfrac{1}{3}T+\tfrac{2}{3}S+2L(1)+2L(3)]+2\ln\left[\frac{m_2}{m_1}\right][L(2)+L(4)]\right]. \tag{2.22}$$

Summing all the diagrams, the fourth-order quark-antiquark potential for different flavors is[23,15]

$$\begin{aligned}\Delta H=&\pi\alpha_{\overline{\rm MS}}(\mu)C_F\left[-\frac{4}{\mathbf{Q}^2}+\frac{(m_1+m_2)^2}{2{m_1}^2{m_2}^2}-\frac{4\mathbf{p}^2}{m_1m_2\mathbf{Q}^2}+\frac{2}{3}\frac{1}{m_1m_2}S+\frac{1}{3}\frac{1}{m_1m_2}T+\frac{4}{m_1m_2}L(1)+\frac{2}{m_1m_2}L(3)\right]\\
&\times\left[1-\frac{\alpha_S}{12\pi}\left[(11C_A-4T_FN_f)\ln\frac{\mathbf{Q}^2}{\mu^2}-\frac{31}{3}C_A+\frac{20}{3}T_FN_f\right]\right]\\
&-\frac{{\alpha_S}^2C_F}{2m_1m_2}\left\{C_A\pi^2\frac{m_1+m_2}{|\mathbf{Q}|}-C_F\frac{2\pi^2m_1m_2}{(m_1+m_2)|\mathbf{Q}|}\right.\\
&\quad+\left[\tfrac{4}{3}(C_A-C_F)+\left[C_F\frac{m_1-m_2}{m_1+m_2}+(\tfrac{1}{2}C_A-C_F)\frac{m_1+m_2}{m_1-m_2}\right]\ln\frac{m_2}{m_1}-\tfrac{7}{6}C_A\ln\frac{\mathbf{Q}^2}{m_1m_2}\right]S\\
&\quad-\tfrac{1}{3}\left[C_A+2C_F+C_A\ln\frac{\mathbf{Q}^2}{m_1m_2}\right]T\\
&\quad\left.-2\left[2C_F+C_A\ln\frac{\mathbf{Q}^2}{m_1m_2}\right][L(1)+L(3)]-2C_A\ln\frac{m_2}{m_1}[L(2)+L(4)]\right\}.\end{aligned} \tag{2.23}$$

III. THE FORM OF THE SPIN-DEPENDENT FORCES

The generalized EFG formalism

The effective potential is obtained by adding together the contributions of all the diagrams. The result is, of course, gauge invariant. To express the result we shall extend the standard formalism of Eichten and Feinberg[10] and Gromes.[12] Their classification of the spin-dependent forces is adequate for expressing the tree-level result but we must extend their formalism to include the one-loop contributions. For unequal masses the result is

$$V(r)=E(r)+\left[\frac{\mathbf{S}_1}{{m_1}^2}+\frac{\mathbf{S}_2}{{m_2}^2}\right]\cdot\mathbf{L}\frac{1}{r}\left[\frac{1}{2}\frac{dE}{dr}(r)+\frac{dV_1}{dr}(m_1,m_2,r)\right]+\left[\frac{\mathbf{S}_1+\mathbf{S}_2}{m_1m_2}\right]\cdot\mathbf{L}\frac{1}{r}\frac{dV_2}{dr}(m_1,m_2,r)$$
$$+\frac{1}{m_1m_2}(\hat{\mathbf{r}}\cdot\mathbf{S}_1\hat{\mathbf{r}}\cdot\mathbf{S}_2-\tfrac{1}{3}\mathbf{S}_1\cdot\mathbf{S}_2)V_3(m_1,m_2,r)+\frac{1}{3}\frac{\mathbf{S}_1\cdot\mathbf{S}_2}{m_1m_2}V_4(m_1,m_2,r)$$
$$+\left[\left[\frac{\mathbf{S}_1}{{m_1}^2}-\frac{\mathbf{S}_2}{{m_2}^2}\right]\cdot\mathbf{L}+\left[\frac{\mathbf{S}_1-\mathbf{S}_2}{m_1m_2}\right]\cdot\mathbf{L}\right]V_5(m_1,m_2,r)\,, \tag{3.1}$$

where $E(r)$ is the static quarkonium potential and V_i, $i=1,\ldots,5$ are the various terms in $V_{\rm SD}$. Also $\mathbf{L}$ is the angular momentum operator. This is the generalized EFG formalism. In perturbative QCD, including the one-loop contribution, we have

$$\bar{E}(r)=-\frac{1}{r}C_F\alpha_{\overline{\rm MS}}(\mu)\left[1+\frac{\alpha_S}{\pi}\left[\frac{b_0}{2}[\ln(\mu r)+\gamma_E]+\tfrac{5}{12}b_0-\tfrac{2}{3}C_A\right]\right],$$
$$V_1(m_1,m_2,r)=-\frac{1}{r}\frac{1}{2}C_F\frac{{\alpha_S}^2}{\pi}(C_F-C_A\{\ln[(m_1m_2)^{1/2}r]+\gamma_E\}),$$
$$V_2(m_1,m_2,r)=-\frac{1}{r}C_F\alpha_{\overline{\rm MS}}(\mu)\left[1+\frac{\alpha_S}{\pi}\left[\frac{b_0}{2}[\ln(\mu r)+\gamma_E]+\tfrac{5}{12}b_0-\tfrac{2}{3}C_A+\tfrac{1}{2}(C_F-C_A\{\ln[(m_1m_2)^{1/2}r]+\gamma_E\})\right]\right],$$
$$V_3(m_1,m_2,r)=\frac{1}{r^3}3C_F\alpha_{\overline{\rm MS}}(\mu)\left[1+\frac{\alpha_S}{\pi}\left[\frac{b_0}{2}[\ln(\mu r)+\gamma_E-\tfrac{4}{3}]+\tfrac{5}{12}b_0-\tfrac{2}{3}C_A\right.\right.$$
$$\left.\left.+\tfrac{1}{2}(C_A+2C_F-2C_A\{\ln[(m_1m_2)^{1/2}r]+\gamma_E-\tfrac{4}{3}\})\right]\right], \tag{3.2}$$
$$V_4(m_1,m_2,r)=8\pi C_F\alpha_{\overline{\rm MS}}(\mu)\left[\left\{1+\frac{\alpha_S}{\pi}\left[\tfrac{5}{12}b_0-\tfrac{2}{3}C_A-C_A+C_F\right.\right.\right.$$
$$\left.\left.-\tfrac{3}{4}\left[C_F\frac{m_1-m_2}{m_1+m_2}+\tfrac{1}{2}(C_A-2C_F)\frac{m_1+m_2}{m_1-m_2}\right]\ln\frac{m_2}{m_1}\right]\right\}\delta^3(r)$$
$$\left.+\frac{\alpha_S}{\pi}\left[-\frac{b_0}{4}\frac{1}{2\pi}\nabla^2\left[\frac{\ln(\mu r)+\gamma_E}{r}\right]+\tfrac{7}{8}C_A\frac{1}{2\pi}\nabla^2\left[\frac{\ln[(m_1m_2)^{1/2}r]+\gamma_E}{r}\right]\right]\right],$$
$$V_5(m_1,m_2,r)=\frac{1}{r^3}\frac{1}{4}C_FC_A\frac{{\alpha_S}^2}{\pi}\ln\frac{m_2}{m_1}\,.$$

Each $V_i(m_1,m_2,r)$ is a gauge-invariant quantity. $\bar{E}(r)$ is the perturbative expression for the spin-independent potential neglecting relativistic corrections. $V_1(m_1,m_2,r)$ is related to the vertex form factor K_1+K_2. $V_4(m_1,m_2,r)$ determines the hyperfine structure while the other $V_i(m_1,m_2,r)$'s contribute to the fine structure. The $V_5(m_1,m_2,r)$ potential is the new one that we have added to the EFG formalism. We note that, for fixed m_1, $V_1(m_1,m_2,r)\to\infty$ as $m_2\to\infty$. The presence of $V_5(m_1,m_2,r)$ precisely cancels this logarithmic divergence, so that $V(r)$ in Eq. (3.1) remains finite. It is possible that further generalizations are needed to describe higher-order terms in perturbation theory. For the equal-mass case the $V_5(m,r)$ term vanishes and the contribution of the annihilation diagrams must be added to $V_4(m_1,m_2,r)$. The generalized EFG formalism for equal masses is now

$$V(r)=E(r)+\frac{1}{m^2}(\mathbf{S}_1+\mathbf{S}_2)\cdot\mathbf{L}\frac{1}{r}\left[\frac{1}{2}\frac{dE}{dr}(r)+\frac{dV_1}{dr}(m,r)+\frac{dV_2}{dr}(m,r)\right]+\frac{1}{m^2}(\hat{\mathbf{r}}\cdot\mathbf{S}_1\hat{\mathbf{r}}\cdot\mathbf{S}_2-\tfrac{1}{3}\mathbf{S}_1\cdot\mathbf{S}_2)V_3(m,r)$$
$$+\frac{1}{3}\frac{\mathbf{S}_1\cdot\mathbf{S}_2}{m^2}V_4(m,r)\ ; \tag{3.3}$$

$$\bar{E}(r)=-\frac{1}{r}C_F\alpha_{\overline{\rm MS}}(\mu)\left[1+\frac{\alpha_S}{\pi}\left[\frac{b_0}{2}[\ln(\mu r)+\gamma_E]+\tfrac{5}{12}b_0-\tfrac{2}{3}c_A\right]\right],$$

$$V_1(m,r)=-\frac{1}{r}\frac{1}{2}C_F\frac{{\alpha_S}^2}{\pi}\{C_F-C_A[\ln(mr)+\gamma_E]\},$$

$$V_2(m,r)=-\frac{1}{r}C_F\alpha_{\overline{\rm MS}}(\mu)\left[1+\frac{\alpha_S}{\pi}\left[\frac{b_0}{2}[\ln(\mu r)+\gamma_E]+\tfrac{5}{12}b_0-\tfrac{2}{3}C_A+\tfrac{1}{2}\{C_F-C_A[\ln(mr)+\gamma_E]\}\right]\right], \tag{3.4}$$

$$V_3(m,r)=\frac{1}{r^3}3C_F\alpha_{\overline{\rm MS}}(\mu)\left[1+\frac{\alpha_S}{\pi}\left[\frac{b_0}{2}[\ln(\mu r)+\gamma_E-\tfrac{4}{3}]+\tfrac{5}{12}b_0-\tfrac{2}{3}C_A+\tfrac{1}{2}\{C_A+2C_F-2C_A[\ln(mr)+\gamma_E-\tfrac{4}{3}]\}\right]\right],$$

$$V_4(m,r)=8\pi C_F\alpha_{\overline{\rm MS}}(\mu)\left\{\left[1+\frac{\alpha_S}{\pi}[\tfrac{5}{12}b_0-\tfrac{11}{12}C_A-\tfrac{1}{2}C_F+\tfrac{3}{2}(1-\ln 2)T_F]\right]\delta^3(r)\right.$$
$$\left.+\frac{\alpha_S}{\pi}\left[-\frac{b_0}{4}\frac{1}{2\pi}\nabla^2\left[\frac{\ln(\mu r)+\gamma_E}{r}\right]+\tfrac{7}{8}C_A\frac{1}{2\pi}\nabla^2\left[\frac{\ln(mr)+\gamma_E}{r}\right]\right]\right\}.$$

The EFG methods start from a $1/m$ expansion for the quark propagator and derive expressions for the spin-dependent parts of the $(Q\bar{Q})$ potential. A glance at the perturbative expression for $V_5(m_1,m_2,r)$ reveals why the EFG method could not include this term. They are proportional to $\ln(m_i)$ which is not analytic as $m_i\to\infty$. This nonanalytic behavior is not confined to $V_5(m_1,m_2,r)$. All of the $V_i(m,r)$'s possess this feature.

The logarithms of the mass are new and unusual terms. In the equal-mass case $V_5(m,r)$ disappears but the other $V_i(m,r)$'s still contain logarithms of $(q/m)^2$. These logarithms are not present in QED since C_A vanishes there. They come from the intermediate and the infrared integration regions of the Feynman diagrams, so the renormalization group can tell us little about them. Since many infrared singularities exponentiate, it is possible that these logarithm terms also exponentiate. However, not all logarithms continue to higher orders. Let us recall that the Bethe logarithm in the Lamb shift of the hydrogen atom appears only at first order and not in higher orders.[24] Thus one cannot draw any conclusion about the behavior of the $\ln(q/m)$ in the $V_i(m,r)$'s without going to higher orders in perturbation theory.

The presence of the $\ln(q/m)$ in the $V_i(m,r)$ proves that these forces are flavor dependent. The energy spectrum of both $(c\bar{c})$ and $(b\bar{b})$ bound states is well described by flavor-independent models of $E(r)$ (e.g., the Richardson potential). Unlike the $V_i(m,r)$, $E(r)$ does not depend on the mass of the fermion in perturbation theory to this order. However, it should not be surprising that the spin-dependent forces are different. Flavor dependence for the spin-dependent forces appears natural since the fermion mass is present in perturbation theory at the tree level as well as at the one-loop level. The EFG formalism defines the $V_i(m,r)$ to remove the known tree-level mass dependence from the spin-dependent forces in the hope that the $V_i(m,r)$ are flavor-independent like $E(r)$. The one-loop corrections show that flavor-independent models for the spin forces are incomplete.

In Ref. 10, the following relation is claimed:

$$V_4(m_1,m_2,r)=2\nabla^2V_2(m_1,m_2,r)\ .$$

At the tree level this identity is satisfied, but at the one-loop level it fails for both equal and unequal masses.

Gromes has derived the relation[12]

$$\frac{d}{dr}[E(r)+V_1(m_1,m_2,r)-V_2(m_1,m_2,r)]=0\ . \tag{3.5}$$

This relation between the spin-averaged potential and the two spin-orbit potentials follows from Lorentz invariance. To see this, one starts with the relative coordinate operator for a two-fermion system[25] correct to order $1/c^2$

$$\mathbf{r}=\mathbf{r}_1-\mathbf{r}_2+\frac{\mathbf{p}_1+\mathbf{p}_2}{2(m_1+m_2)}\times\left[\frac{\mathbf{S}_1}{m_1}-\frac{\mathbf{S}_2}{m_2}\right]. \tag{3.6}$$

Under an infinitesimal boost

$$\mathbf{p}_i\to\mathbf{p}_i-m_i\mathbf{v}\ ,$$
$$\hat{\mathbf{r}}\to\hat{\mathbf{r}}-\frac{(\mathbf{v}\times\mathbf{S}_1)}{2m_1}+\frac{(\mathbf{v}\times\mathbf{S}_2)}{2m_2}\ . \tag{3.7}$$

Substituting this into Eq. (3.1) or (3.3) and requiring invariance under the infinitesimal boost yields Eq. (3.5). The perturbative expressions for $E(r)$, $V_1(m_1,m_2,r)$, and

$V_2(m_1,m_2,r)$ verifies this identity at the tree level and at the one-loop levels, for both the unequal- and the equal-mass cases.

Invariance under infinitesimal boosts is also pertinent to $V_5(m_1,m_2,r)$, the term that we have added to the EFG formalism. The symmetry of Eq. (3.7) dictates that $L(2)$ and $L(4)$ must be described by the same potential factor. This also is verified at the one-loop level and we have incorporated it into our formalism by defining only one new potential.

IV. REVIEW OF FINE STRUCTURE: EXPERIMENT

The m^3S_1 states of heavy-quarkonium decay to the n^3P_J states. This transition is an $E1$ transition and the branching ratio is usually quite substantial. In the past few years the $(b\bar{b})$ states have undergone considerable experimental scrutiny.[26] The masses of the $1P$ states have been determined by CLEO, CUSB, Crystal Ball, and ARGUS.[27–30] The masses of the $2P$ states have been measured by one group, CUSB.[31] There have been many theoretical efforts over the years to calculate the P-state masses. With the recent experimental results the stage is set for a confrontation between theory and experiment.

The P-state data are given in Table I. This table lists the observed photon energies for the transition $2\,^3S_1 \rightarrow 1\,^3P_J + \gamma$. The right-hand column gives the values and errors that will be used for calculations herein.[26] Table II lists the photon energies observed by CUSB for the transition $3\,^3S_1 \rightarrow 2\,^3P_J + \gamma$.

The charmonium system has been studied for many years and the P-state masses are known very precisely. This system is more relativistic than $(b\bar{b})$ and hence predictions for charmonium have greater theoretical uncertainties. The data for the energy-level splittings due to spin effects are given in Table III.[32]

TABLE I. Data (Ref. 26) for the $(b\bar{b})$ transition $2\,^3S_1 \rightarrow 1\,^3P_J + \gamma$. E_γ are the photon energies. The last column gives the average photon energies.

	Group	E_γ (MeV)	E_γ (MeV)
$J=2$	CLEO (Ref. 28)	109.5±0.7±1	
	CUSB (Ref. 27)	108.2±0.3±2	109±1
	ARGUS (Ref. 30)	112.5±1.1±2	
	Crystal-Ball (Ref. 29)	108.2±0.7±4	
$J=1$	CLEO	129.0±0.8±1	
	CUSB	128.1±0.4±3	129±1
	ARGUS	132.5±0.5±2	
	Crystal-Ball	127.1±0.8±4	
$J=0$	CLEO	158.0±0.7±1	
	CUSB	149.4±0.7±5	155±4
	ARGUS	156.0±0.7±2	
	Crystal-Ball	160.0±2.4±4	

TABLE II. Data (Ref. 31) for the $(b\bar{b})$ transition $3\,^3S_1 \rightarrow 2\,^3P_J + \gamma$: $R = (M_2 - M_1)/(M_1 - M_0)$. Here, the systematic uncertainty of R is not included.

J	E_γ (MeV)
2	84.2±0.3±2
1	101.4±0.3±3
0	122.1±0.7±5
	$R = 0.85 \pm 0.04$

V. A PERTURBATIVE ANALYSIS OF THE SPIN SPLITTINGS

Extracting $\Lambda_{\overline{\rm MS}}$

Models of heavy quarkonium start with a nonrelativistic, spin-averaged, Hamiltonian that is solved exactly for wave functions and energy levels:[3–6]

$$H_0 = \frac{p^2}{2m} + E(r) .$$

The spin splittings are small corrections to this Hamiltonian and hence can be treated perturbatively. To leading order[33]

$$\begin{aligned}
M(n^3P_2) &= M_0 + (\tfrac{1}{4})\langle V_S\rangle + (1)\langle V_L\rangle + (-\tfrac{1}{10})\langle V_T\rangle , \\
M(n^3P_1) &= M_0 + (\tfrac{1}{4})\langle V_S\rangle + (-1)\langle V_L\rangle + (\tfrac{1}{2})\langle V_T\rangle , \\
M(n^3P_0) &= M_0 + (\tfrac{1}{4})\langle V_S\rangle + (-2)\langle V_L\rangle + (-1)\langle V_T\rangle , \\
M(n^1P_1) &= M_0 + (-\tfrac{3}{4})\langle V_S\rangle + (0)\langle V_L\rangle + (0)\langle V_T\rangle , \\
M(n^3S_1) - M(n^1S_0) &= \langle V_S\rangle ,
\end{aligned} \tag{5.1}$$

where M_0 is the spin-averaged mass. The potentials are from Eq. (3.3)

$$\begin{aligned}
V_S &= \frac{1}{3}\frac{1}{m^2}V_4(m,r) , \\
V_L &= \frac{1}{m^2}\frac{1}{r}\frac{d}{dr}[\tfrac{1}{2}E(r) + V_1(m,r) + V_2(m,r)] , \\
V_T &= \frac{1}{3}\frac{1}{m^2}V_3(m,r) , \\
\langle 1\rangle &= \int_0^\infty dr\, r^2 R_{nl}^2(r) = 1 ,
\end{aligned} \tag{5.2}$$

TABLE III. Data (Ref. 32) for the $(c\bar{c})$ spin splittings. E_γ refers to the photon energies in the $^3S_1 \rightarrow {}^1S_0$ transitions.

State	M_J (MeV)
$(c\bar{c})\ 1^3P_2$	3555.8±0.6
$(c\bar{c})\ 1^3P_1$	3510.0±0.6
$(c\bar{c})\ 1^3P_0$	3415.0±1.0
State	E_γ (MeV)
$c\bar{c}\ 1S$	113.0±5
$c\bar{c}\ 2S$	92.0±5

and the expectation values are evaluated with respect to the appropriate (n,l) states.

The simple relations of Eqs. (5.1) are not true beyond first order; but higher orders will be smaller by a factor of order $(v/c)^2$. We shall consistently neglect the contribution from higher-order nonrelativistic perturbation theory since relativistic corrections to heavy-quarkonium bound states which are of comparable sizes cannot be completely calculated at the present. We are forced to accept a theoretical uncertainty of order $(v/c)^2$ when calculating any processes involving heavy quarkonium.

Table IV gives typical theoretical values for $\langle V_S \rangle$, $\langle V_L \rangle$, and $\langle V_T \rangle$ using the perturbative calculations. For the P states, δ functions in V_S give no contribution so $\langle V_S \rangle$ is second order in α_S.

For the hyperfine structure the situation is simple. Only one perturbation contributes to the observed mass splitting V_S. The size of the measured fine-structure mass splittings depends on two quantities: $\langle V_L \rangle$ and $\langle V_T \rangle$. The dependence on M_0 and $\langle V_S \rangle$ cancels out when we look at mass differences. To extract $\Lambda_{\overline{\rm MS}}$ from the fine-structure energy-level splittings we first invert Eq. (5.1) to get experimental values for $\langle V_L \rangle$ and $\langle V_T \rangle$. These quantities are extracted from the data because we want to keep the two perturbations separate. The spin-orbit and the tensor terms have different angular dependences and probe slightly different scales. Nonperturbative contributions should be smaller for the potentials that probe shorter-distance scales.

To simplify the analysis we shall first consider the special case where the nonperturbative contributions are taken to be zero. By using the one-loop perturbative expressions to describe the V we reduce the number of unknown parameters to one, namely, $\Lambda_{\overline{\rm MS}}$, the QCD scale parameter. $\Lambda_{\overline{\rm MS}}$ can then be extracted from the data for the spin-dependent level splittings of heavy quarkonium. All other quantities that the spin splittings depend on, like the quark mass and the wave function, can be determined from other properties of the heavy-quarkonium spectrum. The validity and accuracy of the perturbative expressions can be checked *a posteriori* by comparing the values of $\Lambda_{\overline{\rm MS}}$ from several different spin splittings.

Using the perturbative expression for V we then have a quadratic equation in $\alpha_{\overline{\rm MS}}(\mu)$. The coefficients of $\alpha_{\overline{\rm MS}}$ depend on μ and the integrals over quarkonium wave functions while the constant part is determined from experiment. After choosing a prescription to specify μ and using a nonrelativistic quarkonium model to calculate wave-function factors we then solve for $\alpha_{\overline{\rm MS}}(\mu)$. A sample calculation is shown in Appendix C.

The relation between the $\Lambda_{\overline{\rm MS}}$ parameter and the coupling constant is taken to be the integral of the two-loop β function with three flavors:[5,7,34]

TABLE IV. Typical theoretical values for $\langle V_S \rangle$, $\langle V_L \rangle$, and $\langle V_T \rangle$. The perturbative QCD expressions for the V's are used with the patched potential and, where applicable, the Grunberg prescription. Here $\Lambda_{\overline{\rm MS}}=0.30$ GeV is used.

State	$\langle V_S \rangle$ (MeV)	$\langle V_L \rangle$ (MeV)	$\langle V_T \rangle$ (MeV)
$(c\bar{c})$ $1S$	101.0	0.0	0.0
$(c\bar{c})$ $2S$	69.0	0.0	0.0
$(c\bar{c})$ $1P$	−3.6	48.0	46.0
$(b\bar{b})$ $1S$	35.0	0.0	0.0
$(b\bar{b})$ $2S$	19.0	0.0	0.0
$(b\bar{b})$ $3S$	15.0	0.0	0.0
$(b\bar{b})$ $1P$	−0.4	13.0	9.0
$(b\bar{b})$ $2P$	−0.3	9.3	6.7

TABLE V. Fitting the fine structure with the one-loop perturbative expression. The fourth column gives the size of the one-loop correction in the BLM prescription. The long-range contributions are taken to be zero; $N_F=3$; * implies that no value fits the data. (a) The BGT potential. (b) The patched potential.

	BLM			Grunberg	
State	μ (GeV)	$\Lambda_{\overline{\rm MS}}$ (MeV)	Corr. (percent)	μ (Gev)	$\Lambda_{\overline{\rm MS}}$ (MeV)
		(a)			
$c\bar{c}$ $1P$ spin-orbit	0.484	220.0±3	−30.0	0.704	209.0±3
$c\bar{c}$ $1P$ tensor	0.676	316.0±4	+18.0	0.544	291.0±4
$b\bar{b}$ $1P$ spin-orbit	0.868	*		1.65	288.0±40
$b\bar{b}$ $1P$ tensor	1.21	279.0±148	−9.0	1.46	282.0±150
$b\bar{b}$ $2P$ spin-orbit	1.07	484.0±274	−44.0	1.85	379.0±94
$b\bar{b}$ $2P$ tensor	1.49	288.0^{+289}_{-270}	−22.0	1.57	289.0^{+297}_{-279}
		(b)			
$c\bar{c}$ $1P$ spin-orbit	0.476	208.0±3	−28.0	0.688	200.0±3
$c\bar{c}$ $1P$ tensor	0.665	304.0±5	+18.0	0.515	272.0±4
$b\bar{b}$ $1P$ spin-orbit	0.846	*		1.62	297.0±39
$b\bar{b}$ $1P$ tensor	1.18	289.0±148	−10.0	1.44	292.0±151
$b\bar{b}$ $2P$ spin-orbit	1.04	*		1.82	394.0±95
$b\bar{b}$ $2P$ tensor	1.45	301.0^{+287}_{-282}	−28.0	1.54	302.0^{+294}_{-281}

TABLE VI. The hyperfine splittings using the order α_S^2 perturbative expressions. We solve for $\Lambda_{\overline{\rm MS}}$; $N_F=3$. The fourth column gives the size of the one-loop correction in the BLM prescription. * implies that no values fit the data. (a) The BGT potential. (b) The patched potential.

	BLM			Grunberg	
State	μ (GeV)	$\Lambda_{\overline{\rm MS}}$ (MeV)	Corr. (percent)	μ (GeV)	$\Lambda_{\overline{\rm MS}}$ (MeV)
		(a)			
$c\bar{c}$ 1S	0.848	335.0±27	−27.0	1.25	320.0±24
$c\bar{c}$ 2S	1.05	420.0±28	−10.0	1.21	428.0±28
		(b)			
$c\bar{c}$ 1S	0.774	*		1.23	358.0±24
$c\bar{c}$ 2S	0.970	445.0±28	−16.0	1.18	451.0±29

$$\rho=\frac{\alpha_{\overline{\rm MS}}(Q)}{4\pi}\ ,$$

$$\ln\frac{Q^2}{\Lambda_{\overline{\rm MS}}{}^2}=\frac{1}{b_0\rho}+\frac{b_1}{b_0{}^2}\ln\left[\frac{b_0\rho}{1+\frac{b_1}{b_0}\rho}\right]\ , \tag{5.3}$$

$$b_0=\tfrac{11}{3}C_A-\tfrac{4}{3}T_FN_f\ ,$$

$$b_1=\tfrac{34}{3}(C_A)^2-\tfrac{20}{3}C_AT_FN_f-4C_FT_FN_f\ .$$

The general forms for C_A and T_F are given below Eq. (2.6) for SU(N). For QCD with three light flavors ($N_f=3$), $b_0=9$ and $b_1=64$.

The values of $\Lambda_{\overline{\rm MS}}$ extracted from the spin splittings are given in Tables V and VI and shown in Fig. 1. Two prescriptions for choosing μ have been used in Tables V and VI. For the moment, let us concentrate on the results from just one of them, the Grunberg prescription (see Appendix A). Each energy-level difference yields one value for $\Lambda_{\overline{\rm MS}}$ so the fine structure of a state yields two values while the hyperfine structure yields one. Figure 1 displays these results with error bars that are the experimental errors from the photon energies. Here we use the quarkonium potential proposed by Richardson,[4] Buchmüller, Grunberg, and Tye,[5] and Buchmüller and Tye[6] to be referred to as the RBGT potential. Since only the difference of energy levels is used in computing $\Lambda_{\overline{\rm MS}}$ some of the systematic experimental error should cancel out and the error bars shown in Fig. 1 are probably too large. We will try to point out the different possible sources of theoretical errors and their effects.

Theoretical uncertainties

One of the largest potential sources of error is from order $(v/c)^2$ corrections to the perturbative expressions. Another source of error could come from nonperturbative contributions. These corrections should be larger for $(c\bar{c})$ than for $(b\bar{b})$ but it is impossible to completely calculate them at the present time. Both of the above sources of error should, in principle, contribute with signs and magnitudes that are uncorrelated for the different perturbative expressions. It has been argued previously herein that these effects should not be large and we can see this from Fig. 1. The fluctuations of $\Lambda_{\overline{\rm MS}}$ are not large and lie within the present experimental errors of $(b\bar{b})$ data but not within that of the precise $(c\bar{c})$ data. Naively the expected theoretical fluctuations for $(b\bar{b})$ values should be smaller than those of $(c\bar{c})$ values. Improved data on the $(b\bar{b})$ spin splittings are needed before this could be observed.

Besides the fluctuating sources of errors, overall shifts of the values are possible. The most likely source of any such theoretical errors will be in the wave-function-dependent factor. The accuracy of this factor is discussed in the next section where we estimate the uncertainty to be 15%. Because the spin splittings all depend on just one power of α_S at the tree level, the relative error in α_S is of similar size. The error in Λ is determined by the β function

$$\frac{1}{2}\frac{d\rho}{\rho}\left[\frac{1}{-b_0\rho-b_1\rho^2}\right]=\frac{d\Lambda}{\Lambda}\ . \tag{5.4}$$

For the fine structure of $(b\bar{b})$ the average α_S is 0.30. Using Eq. (5.4) an uncertainty in the wave-function factor of 15% yields a relative uncertainty in $\Lambda_{\overline{\rm MS}}$ of 30% for the $(b\bar{b})$ fine structure. For charmonium the coupling constant is larger and the uncertainty from this source is smaller. Because the values of the coupling constant are relatively large the sensitivity to the wave-function-dependent factors is reduced from what one might naively expect.

As argued above from Eq. (5.4), when the coupling constant is large, the sensitivity to Λ is also large. However, when the coupling constant is large, results are sensitive to details such as the choice of the renormalization scheme and the prescription. In order to examine this problem we have calculated all results with two different prescriptions.

Our first approach is to fix μ by requiring the one-loop correction term to vanish. This incorporates all of the correction term into the coupling constant and, in effect, the particular process under consideration becomes a physical definition of the coupling constant. This approach has been advocated by Grunberg.[35] The other prescription that we use is to take the Brodsky, Lepage, and Mackenzie[36] (BLM) prescription with the $\overline{\rm MS}$ definition of the coupling constant (see Appendix A). This

prescription takes parts of the one-loop correction term that are known to be present to all others in perturbation theory and incorporates them in the coupling constant. The $\overline{\text{MS}}$ scheme is known to be close to a physical definition of the coupling constant and is convenient for perturbative calculations.

The two approaches yield similar results when the size of the correction term in the BLM prescription is small, i.e., less than about 30%. When the BLM correction term is larger than this the results are dissimilar and there are two possible interpretations. One is that no expansion in α_S can describe the process accurately. The other interpretation is that the $\overline{\text{MS}}$ scheme is not sufficiently close to the proper physical scheme to judge whether the expansion in α_S is valid. A different definition of the coupling constant where the correction term was small might then be more appropriate. When the correction term in the BLM prescription is large one cannot always fit the perturbative expression to the data (see Table V). To avoid these problems we have plotted, in Fig. 1, $\Lambda_{\overline{\text{MS}}}$ using the Grunberg prescription. The success of perturbation theory can then be judged by the fluctuations of the results. This method is not sensitive to the correct definition of the coupling constant.

The eight values of $\Lambda_{\overline{\text{MS}}}$ in Fig. 1 are consistent with each other within the experimental and theoretical uncertainties. Nonperturbative effects are expected to cause some fluctuations. The charmonium values fluctuate around the mean by about 75 MeV while the $(b\bar{b})$ fluctuations should be smaller and are all within the present experimental errors. Overall shifts of the values from uncertainties in the wave function are possible. These should be largest for $(b\bar{b})$ where we estimate the corresponding uncertainty in $\Lambda_{\overline{\text{MS}}}$ to be 20–30%. From the above considerations we obtain (to be discussed later)

$$\Lambda^{(3)}_{\overline{\text{MS}}}=0.30\pm0.06 \text{ GeV} .$$

This value is consistent with other, independent determinations of $\Lambda_{\overline{\text{MS}}}$. (See *Note added* where the analysis is updated.)

Accuracy of perturbative coefficients

The nonrelativistic models of heavy quarkonium allow one to calculate the wave functions of the bound states. This gives us the factors needed in the spin splittings. However, it must be noted that most phenomenological potentials will not accurately describe the QCD static potential at the distance scales that contribute most to the spin splittings. The phenomenological potentials are defined to fit the spin-averaged energy-level spectrum of heavy quarkonium and are most accurate at these longer-distance scales.

Since the spin-averaged potential is only known phenomenologically at the scales of the bound states there will be some error in the potential and consequently also in the wave functions. Theoretical uncertainties can be large for some processes that are sensitive to small changes. An example of this is the $E1$ transition amplitude which is proportional to the overlap of two different wave functions often with differing numbers of radial nodes. In some cases this overlap changes drastically when small changes are made in the wave functions.[13,14] On the other hand, the expectation values of Eqs. (5.1) are between the same wave function. Errors in the energy levels from using these wave functions in nonrelativistic perturbation theory will be the square of the error in the wave function. This fact is used in the variational method to obtain accurate energy-level estimates from crude wave functions. Applied here, it shows that the size of $\langle V \rangle$ will be sensitive to what one uses for V, not to the wave function.

The BGT potential[5,6] incorporates the QCD perturbative expression for the potential at short distances and is numerically equivalent for the $(c\bar{c})$ and $(b\bar{b})$ systems to that proposed by Richardson.[4] This RBGT potential fits the energy spectra extremely well (within 10 MeV) and *a priori* is a prime choice for yielding good wave functions and accurate values for the wave-function-dependent factors. Unfortunately, the BGT potential is consistent with a value of $\Lambda_{\overline{\text{MS}}}=0.50$ GeV at short distances which is larger than the data indicate. To remedy this we have constructed a potential by patching the perturbative expression for $E(r)$ [Eq. (3.4)] with $\Lambda_{\overline{\text{MS}}}=0.30$ GeV onto the RBGT potential (see Appendix B). The BLM prescription is used to fix μ and Eq. (5.3) is used to find the size of the coupling constant. By requiring the potential and its first derivative to be continuous the patching point is determined to be 0.14 fm. The wave-function factors necessary for the spin splittings, as calculated in the BGT potential and in the patched potential, are given in Table VII.

The accuracy of the wave-function factors can be tested empirically using experimental data from quarkonium decay rates. The hyperfine splitting depends on the wave function at the origin in the tree level and heavy-quarkonium decay rates also have this same wave-function factor. Table VIII compares experimental widths to the predicted widths using the one-loop corrections and the wave functions calculated from the RBGT and patched potentials. Instead of trying to extract a value for the Λ parameter from the data, the accuracy of the wave function at the origin will be assessed.

The data for the leptonic widths are the most precise and provide potentially the best information on the wave-function-dependent factors. At the tree level the expression is independent of QCD but a large order-α_S correction enters at the one-loop level:

$$\Gamma(n^3S_1\to l^+l^-)=4\frac{|R_n(0)|^2}{M^2}q^2\alpha^2\left[1-\frac{16}{3}\frac{\alpha_{\overline{\text{MS}}}(\mu)}{\pi}\right] . \tag{5.5}$$

The size of the coupling constant to take in this correction term is unknown since the next-order corrections have not been calculated but μ must be chosen in a consistent manner. Table VIII shows the comparison between theory and experiment.

The theoretical wave-function factors from the BGT and patched potentials fit the experimental data[32] if we choose the Grunberg renormalization points appropriately. In choosing the relation between μ and the bound-state mass, errors from overall shifts of the wave-function

TABLE VII. Some wave-function-dependent numbers pertinent to the spin splittings as calculated in two different potentials. We use the normalization $\langle 1 \rangle = \int_0^\infty dr\, r^2 R_n^2(r) = 1$. (a) The BGT potential. (b) The patched potential.

m_Q (GeV)	n	P states $\left\langle \frac{1}{r^3} \right\rangle$ (GeV^3)	P states $\left\langle \frac{\ln(mr)}{r^3} \right\rangle$ (GeV^3)	S states $\lvert R_n(0) \rvert^2$ (GeV^3)	S states $\left\langle \frac{1}{2\pi} \nabla^2 \left[\frac{\ln(mr)+\gamma_E}{r} \right] \right\rangle$ (GeV^3)
			(a)		
1.48	1	0.0987	0.0699	0.791	0.435
1.48	2	0.0862	0.0415	0.514	0.500
4.88	1	0.525	0.690	6.13	−1.75
4.88	2	0.406	0.451	3.05	0.133
4.88	3	0.356	0.354	2.33	0.442
30.0	1	11.8	24.2	266.0	−324.0
30.0	2	7.05	13.2	81.4	−80.7
40.0	1	20.9	44.6	513.0	−687.0
40.0	2	11.9	23.5	145.0	−164.0
50.0	1	32.9	72.5	861.0	−1232.0
50.0	2	18.1	37.0	231.0	−282.0
60.0	1	48.2	109.0	1320.0	−1980.0
60.0	2	25.7	54.0	340.0	−442.0
			(b)		
1.44	1	0.0947	0.0659	0.689	0.294
1.44	2	0.0828	0.0389	0.456	0.400
4.84	1	0.504	0.673	4.66	−2.48
4.84	2	0.388	0.438	2.50	−0.385
4.84	3	0.339	0.344	1.96	0.027
30.0	1	8.15	17.9	156.0	−228.0
30.0	2	5.40	10.8	68.0	−82.9
40.0	1	13.0	30.1	310.0	−482.0
40.0	2	8.95	19.0	119.0	−159.0
50.0	1	19.1	45.8	537.0	−875.0
50.0	2	13.6	29.9	180.0	−257.0
60.0	1	26.7	65.5	850.0	−1433.0
60.0	2	19.4	43.7	251.0	−376.0

factors are partially absorbed. The wave-function factors calculated from the patched potential are consistently smaller because we have made the potential shallower by decreasing $\Lambda_{\overline{\rm MS}}$. Such overall shifts are the largest theoretical uncertainty in the value of $\Lambda_{\overline{\rm MS}}$ that we extract for the spin splitting data. As an estimate of the magnitude of the theoretical uncertainty of our spin splitting analysis to overall shifts we take the shift of the $(c\bar{c})$ S-state wave-function factors in Table VII. These are the largest shifts that are pertinent to extracting $\Lambda_{\overline{\rm MS}}$ and are between 10—15%.

The value of $\lvert \Psi_\Upsilon(0) \rvert^2$ is 2.3 times greater when calculated from the Coulomb plus linear potential with the parameter set of Eichten *et al.* [Ref. 3 (1980)] than from the RBGT potential. In Table IX, the wave-function factors for P-state decay are given for the two models. The models disagree less for P states since the centrifugal term in Schrödinger's equation dominates at short distances where the two potentials differ. Because of the centrifugal term the P-state wave-function factors are more model independent than the S-state factors and probably more accurate. The S-state factors were accurate within the uncertainties so the P-state factors should also be accurate within an uncertainty of 10—15%.

The hadronic decay widths of the P states have been calculated[37] in Table IX from the RBGT wave-function factor using $\Lambda_{\overline{\rm MS}}=0.30\pm0.06$ GeV and the Grunberg prescription. For the 1^{++} and 1^{+-} states the one-loop correction is not known so the coupling constant was taken to be $\alpha_S=0.24\pm0.05$. This number is the average, and the deviation is half the difference of the coupling con-

TABLE VIII. Partial widths of the 1^{--} states (Ref. 32). Testing the wave function at the origin. μ is chosen to fit the data. $\Lambda_{\overline{\rm MS}}=300$ MeV, $N_F=3$.

Width	Expt. (keV)	Theoretical (keV) BGT $\mu=2M/3$	Theoretical (keV) Patched $\mu=2M$
$\Gamma_{e^+e^-}(b\bar{b}\ 1S)$	1.10±0.12	1.13	0.94
$\Gamma_{e^+e^-}(b\bar{b}\ 2S)$	0.507±0.051	0.50	0.45
$\Gamma_{e^+e^-}(b\bar{b}\ 3S)$	0.362±0.050	0.36	0.33
$\Gamma_{e^+e^-}(c\bar{c}\ 1S)$	4.60±0.39	4.3	4.7
$\Gamma_{e^+e^-}(c\bar{c}\ 2S)$	2.05±0.21	2.1	2.3

TABLE IX. $(b\bar{b})$ P-state decay. $\Lambda_{\overline{\rm MS}}=300\pm60$ MeV; $N_F=3$; * implies these numbers were not calculated in Kuang and Yan (Ref. 3). Misprints in Table III of Ref. 3 have been corrected.

	$\lvert R'_n(0)\rvert^2$ (GeV^5)			Gluon annihilation width (keV)	
State	Cornell (Ref. 3) potential	Richardson potential	BGT potential	Cornell (Ref. 3) potential	RBGT potential
$1\,^3P_2$				160.0	135.0±15
$1\,^3P_1$	2.2	1.47	1.42	60.0	80.0±50
$1\,^3P_0$				600.0	1250.0±250
$1\,^1P_1$				40.0	70.0±40
$2\,^3P_2$				200.0	130.0±15
$2\,^3P_1$	2.6	1.65	1.62	80.0	80.0±50
$2\,^3P_0$				760.0	1250.0±250
$2\,^1P_1$				*	70.0±40
$3\,^3P_2$				*	130.0±15
$3\,^3P_1$	*	1.77	1.75	*	80.0±50
$3\,^3P_0$				*	1250.0±250
$3\,^1P_1$				*	70.0±40

stants predicted for 2^{++} and 0^{++} hadronic decay by the Grunberg prescription. Table IX also contains the older predictions of the Coulomb plus linear potential.[3]

Comments on coupled channel effects

The light quarks profoundly influence the heavy-quark spectrum. Above the threshold energy for producing heavy-light mesons, the heavy-quark states are very broad because of the strong decay $(Q\bar{Q})\rightarrow(Q\bar{q})+(q\bar{Q})$. Attempts to incorporate this strong decay process into the potential model for heavy quarkonium usually go under the title of "coupled channel analysis." Here we wish to express our viewpoint on what these analyses accomplish and their relevance to our calculation.

Coupled channel analyses usually start with free, uncoupled quarkonium states and then add an interaction term to the Hamiltonian that couples the $(Q\bar{Q})$ states to the $(Q\bar{q})+(q\bar{Q})$ hadron-hadron states. This allows the decay of the heavy-quark states but also, at second order in perturbation theory, this additional term produces corrections to the masses. After folding these mass shifts in, the new heavy-quarkonium states contain a small light-quark content in the form of virtual $(Q\bar{q})+(q\bar{Q})$ states.

Coupled channel analyses typically suffer from several problems. There is little theoretical input from QCD on the proper form of the interaction Hamiltonian that couples the $(Q\bar{Q})$ and $(Q\bar{q})+(q\bar{Q})$ states. Also the light-heavy states are relativistic states and hence not accurately described by the Schrödinger equation. Because of these problems different coupled channel analyses usually agree only to sign and magnitude of mass shifts. After renormalizing the $1S$ states to fit the data, the resulting mass shifts for states below threshold are very small (≤ 10 MeV) and different analyses do not even agree in the sign.

In our viewpoint, for the spin-averaged heavy-quarkonium states far below threshold, adding a virtual $(Q\bar{q})+(q\bar{Q})$ content to the $(Q\bar{Q})$ states is equivalent to adding light-quark pair effects (i.e., vacuum polarization) to $E(r)$, the heavy-quarkonium potential. Perturbative QCD can accurately tell us the light-quark behavior of $E(r)$, far below threshold. At and above threshold perturbative QCD is not valid and coupled channel analyses provide the best indication of light-quark effects. For the spin-dependent forces, the light-quark pair vacuum polarization is included.

Some simple observations can be made that support this viewpoint. Introducing a continuum of $(Q\bar{Q})$ states into the heavy-quark model without introducing light quarks can be simply accomplished by setting the potential equal to a constant at the threshold. Doing this for $(b\bar{b})$ and $(c\bar{c})$, the discrete states below threshold are shifted by less than 1 MeV. The form of the potential is such that states far below threshold are very insensitive to threshold effects. What causes the large mass shifts of these states in coupled channel analyses is probably not the existence of thresholds but the addition of light quarks.

Further insight can be gained from perturbative QCD. Equations (3.4) tell us that the addition of light quarks makes the potential steeper at short distances. With an increase in flavor, states far below threshold will decrease in mass and the size of the change will be of the order of tens of MeV. This is qualitatively in agreement with the predictions of coupled channel analyses.[9]

In summary, coupled channel analyses attempt to include effects of light quarks into the heavy-quark model. For our purpose, we feel that this can be done most accurately for states far below threshold by including vacuum polarization effects into the heavy-quarkonium potential. For our spin-splittings analysis we use the experimental data involving states below threshold, and a potential consistent with perturbative QCD and three light flavors.

VI. DISCUSSIONS

A. Scale of the spin-dependent forces

Bound states depend on more than one length scale. The two physical scales pertinent to properties of heavy quarkonium are $\Lambda_{\overline{\rm MS}}$ and the mass of the quark. These two scales are apparent in the perturbative expression for

the $V_i(m,r)$'s since m and α_S appear explicitly.

The renormalization point μ appears in the perturbative expression for the $V_i(m,r)$'s. If the $V_i(m,r)$'s were known to all orders in perturbation theory they would be independent of μ. Since we are forced to work to finite order in α_S we must choose a sensible value for μ. To minimize the contribution of higher orders in α_S we should choose μ such that the μ-dependent terms in the coefficients of α_S^n are small. This means choosing μ, roughly the typical scale of the process, so that the $\ln(q/\mu)$'s are of order 1. Various prescriptions for choosing μ have been proposed and here we use the Grunberg and the BLM prescriptions. The prescriptions provide a framework to judge the validity of perturbation theory for the spin splittings.

To judge *a priori* the validity of a perturbative expression we can use the prescription to determine the typical scale and compare this to Λ. As an example let us apply

TABLE X. The scale of the bound state as given by the prescriptions. The BGT potential is used.

State	Quark mass (GeV)	$\mu_{\rm BLM}$ (GeV)	$\mu_{\rm Grunberg}$ (GeV)
$c\bar{c}$ $1S$	1.48	0.211	0.329
$c\bar{c}$ $2S$	1.48	0.150	0.234
$b\bar{b}$ $1S$	4.88	0.407	0.635
$b\bar{b}$ $2S$	4.88	0.256	0.399
$Q\bar{Q}$ $1S$	30.0	0.683	1.07
$Q\bar{Q}$ $2S$	30.0	0.492	0.767
$Q\bar{Q}$ $1S$	40.0	0.814	1.27
$Q\bar{Q}$ $2S$	40.0	0.573	0.894
$Q\bar{Q}$ $1S$	50.0	0.937	1.46
$Q\bar{Q}$ $2S$	50.0	0.648	1.01
$Q\bar{Q}$ $1S$	60.0	1.06	1.65
$Q\bar{Q}$ $2S$	60.0	0.720	1.12

TABLE XI. Predictions for the spin splittings of $(b\bar{b})$ states. The one-loop perturbative corrections are used to calculate the fine structure and hyperfine structure. In the perturbation we take $\Lambda_{\overline{\rm MS}}=300\pm60$ MeV, $N_F=3$. The fifth column gives the one-loop correction in the BLM prescription. R is given by $R=(M_2-M_1)/(M_1-M_0)$. (a) The BGT potential. (b) The patched potential.

	BLM				Grunberg		
State	μ (GeV)	R	M_1-M_0 (MeV)	Corr. (percent)	μ (GeV)	R	M_1-M_0 (MeV)
			(a)				
$b\bar{b}$ $1P$ spin-orbit	0.868	0.690	25.2±1.6	−39.0	1.65	0.763	26.5±1.9
$b\bar{b}$ $1P$ tensor	1.21			−9.0	1.46		
$M_Q=4.88$ GeV							
$b\bar{b}$ $2P$ spin-orbit	1.07	0.720	19.1±1.2	−29.0	1.85	0.753	19.6±1.3
$b\bar{b}$ $2P$ tensor	1.49			−2.0	1.57		
$M_Q=4.88$ GeV							

State	μ (GeV)	ΔE (MeV)	Corr. (percent)	μ (GeV)	ΔE (MeV)
$b\bar{b}$ $1S$	1.84	41.0±2	−35.0	4.41	46.0±3
$M_b=4.88$ GeV					
$b\bar{b}$ $2S$	2.17	22.0±1	−25.0	4.29	23.0±1
$M_b=4.88$ GeV					
$b\bar{b}$ $3S$	2.33	17.0±1	−21.0	4.24	18.0±1
$M_b=4.88$ GeV					

			(b)				
$b\bar{b}$ $1P$ spin-orbit	0.846	0.682	24.8±1.5	−41.0	1.62	0.764	26.2±1.9
$b\bar{b}$ $1P$ tensor	1.18			−10.0	1.44		
$M_Q=4.84$ GeV							
$b\bar{b}$ $2P$ spin-orbit	1.04	0.716	18.8±1.2	−31.0	1.82	0.751	19.3±1.3
$b\bar{b}$ $2P$ tensor	1.45			−3.0	1.54		
$M_Q=4.84$ GeV							

State	μ (GeV)	ΔE (MeV)	Corr. (percent)	μ (GeV)	ΔE (MeV)
$b\bar{b}$ $1S$	1.61	30.0±1	−43.0	4.46	35.0±2
$M_b=4.84$ GeV					
$b\bar{b}$ $2S$	1.95	18.0±1	−31.0	4.33	19.0±1
$M_b=4.84$ GeV					
$b\bar{b}$ $3S$	2.12	14.0±1	−26.0	4.26	15.0±1
$M_b=4.84$ GeV					

this test to the spin-independent spectrum. From Table X we see that values of μ for $\bar{E}(r)$ are comparable to $\Lambda_{\overline{\rm MS}}$ for $(c\bar{c})$ and $(b\bar{b})$ states. Thus, to describe these spin-independent splittings, the range over which $E(r)$ must be accurate extends heavily into the region where the perturbative expression is no longer convergent. Perturbation theory alone is inadequate in describing the spin-average potential. To remedy this, one adjusts by hand the long-distance behavior of $E(r)$ until it does successfully describe the energy levels. Strong-coupling theory tells us that at long distances the quarkonium potential should be linear in r. Spin-independent potentials proportional to $1/r$ at short distances and r at long distances successfully describe the heavy-quarkonium spectrum.

For the spin-dependent forces, the perturbative expression has a better chance of succeeding alone. From Tables X and XI we see (from the μ's) that for $(c\bar{c})$ and $(b\bar{b})$ the typical distance scales of the spin splittings are much shorter than the scales of the spin-independent spectrum and $\Lambda_{\overline{\rm MS}}$. For the fine structure this is because the tree-level distance dependence, $1/r^3$, weights short distances more heavily in the $\ln(mr)$ terms than does the tree-level dependence $1/r$ of the spin-averaged potential. The same is true for the hyperfine splitting, shorter distances are more important. The spin-dependent forces are relativistic corrections to the spin-averaged forces and because of this probe shorter distances. Thus, to describe the $(b\bar{b})$ and $(c\bar{c})$ spin-dependent splittings, the range over which the $V_i(m,r)$'s must be accurate lies more in the perturbative region than it does for the spin-independent splittings. We expect long-range effects to be less important.

B. The spin-orbit interactions

At present there does not exist a comprehensive, *a priori* calculation of long-range terms in the spin-dependent splittings. For the spin-orbit interaction we do have some clues as to the long-range behavior. There the EFG formalism and the Gromes relation provide us with a framework for making some quantitative estimates. We take several types of long-range contributions and calculate the spin-orbit $\Lambda_{\overline{\rm MS}}$ for each case.

The EFG formalism includes the spin-independent potential $E(r)$ in the expression for the spin-orbit interaction [Eq. (3.3)]. Since the long-range contribution to $E(r)$ is known phenomenologically, this gives us some input as to the long-range behavior of the spin-orbit interaction. The spin-dependent potentials are proportional to $1/r^3$ at short distances. The presence of $E(r)$ implies that the long-distance behavior should be proportional to $1/r$, larger by two powers of r from the short-distance expression. These long-range corrections to the static potentials are only part of the possible nonperturbative contributions but have been the subject of much discussion. Here we wish to discuss the effects of such contributions and what the data imply (a review of other analyses is given in Sec. VII).

The size of the long-range part in the $V_i(m,r)$'s is unknown but we do have one constraint. The Gromes relation [Eq. (3.5)], which follows from Lorentz invariance, tells us that $V_1(m,r)$ and/or $V_2(m,r)$ must contain some long-range contribution similar to $E(r)$. For the spin-orbit force the interaction depends on the three potentials that appear in the Gromes relation. With $E^N(r)$, the nonperturbative part of $E(r)$, approximately known, we need one assumption in order to fully determine the long-range part of the spin-orbit interaction. We will discuss the following four representative cases (other cases can be considered in a similar manner): (1) $V_1^N=-3V_2^N=-\frac{3}{4}E^N$ such that there are no nonperturbative spin interactions (the superscript N denotes nonperturbative, $E^N=E-\bar{E}$); (2) $V_2^N=0$; (3) $V_1^N=0$; (4) $V_1^N=-V_2^N=-\frac{1}{2}E^N$. For each case, three independent determinations of the $\Lambda_{\overline{\rm MS}}$ parameter can be made from the current data on the fine structures from the J/Ψ and Υ systems. Irrespective of which type of long-range spin-orbit interaction one considers, the current data on the V_S and V_T terms provide five more determinations of the $\Lambda_{\overline{\rm MS}}$ parameters. Consistency demands that for one particular type of long-range spin-dependent force we obtain a common value of $\Lambda_{\overline{\rm MS}}$ (within errors). We emphasize that, in contrast with the usual approach which assumes a certain form of the long-range spin force and then confronts experimental data, we use the data to extract the $\Lambda_{\overline{\rm MS}}$ parameter and deduce the long-range spin-dependent potentials.

Now we consider the four types of long-range spin interactions separately.

Case (1): $V_1^N=-3V_2^N=-\frac{3}{4}E^N$ such that $V_{\rm SD}$ is taken entirely to be the expression given by the perturbative QCD calculations. For this case the spin-orbit potential is given by

$$V_L(m,r)=\frac{2}{m^2r^3}\alpha_{\overline{\rm MS}}(\mu)\left[1+\frac{\alpha_S}{\pi}A\right],$$
$$A=\tfrac{1}{2}b_0[\ln(\mu r)+\gamma_E-1]+\tfrac{5}{12}b_0-2+\{\tfrac{8}{9}-2[\ln(mr)+\gamma_E-1]\}. \tag{6.1}$$

By using Eq. (6.1) for V_L we are left with $\alpha_{\overline{\rm MS}}(\mu)$ as the only unknown parameter.

Case (2): $V_2^N=0$ so that $V_1^N=-E^N$. This case is equivalent to the assumption that the spin-averaged confining potential comes from an attractive scalar exchange.[11,12] A phenomenological expression for $E(r)$ (which is consistent with $\Lambda_{\overline{\rm MS}}=0.30$ GeV at short distances) is used to add a long-range part to the interaction:

$$V_L(m,r)=-\frac{1}{2}\frac{1}{m^2r}\frac{dE}{dr}(r)+\frac{8}{3}\frac{1}{m^2r^3}\alpha_{\overline{\rm MS}}(\mu)\left[1+\frac{\alpha_S}{\pi}C\right],$$
$$C=\tfrac{1}{2}b_0[\ln(\mu r)+\gamma_E-1]+\tfrac{5}{12}b_0-2+\tfrac{3}{4}\{\tfrac{8}{9}-2[\ln(mr)+\gamma_E-1]\}. \tag{6.2}$$

We extract $\Lambda_{\overline{\rm MS}}$ from the remaining perturbative, non-phenomenological part of the expression. The results are shown in Fig. 3.

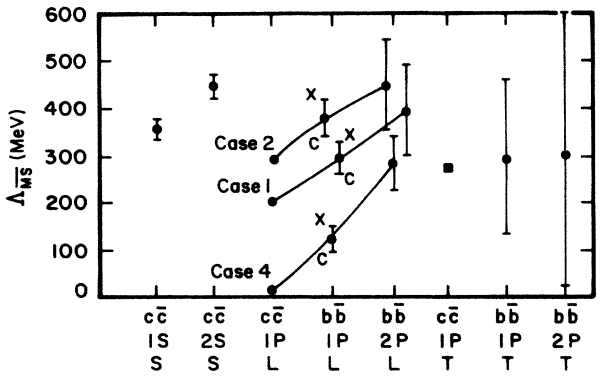

FIG. 3. We extract $\Lambda_{\overline{MS}}$ with several possible long-range forces added to the spin-orbit potential, as explained in the text. The X stands for the data from the Crystal Ball Collaboration (Ref. 29) and the C stands for the data from CUSB (Ref. 27). The spin-spin, spin-orbit, and tensor terms are denoted by S, L, and T, respectively. The spin-independent potential $[E(r)]$ used is consistent with $\Lambda_{\overline{MS}}=0.30$ GeV at short distances.

Case (3): $V_1^N=0$ so that $V_2^N=E^N$. For this case

$$V_L(m,r)=\frac{1}{m^2r}\frac{d}{dr}[\tfrac{3}{2}E+(-\bar{E}+V_1+V_2)] . \quad (6.3)$$

But the combination $(-\bar{E}+V_1+V_2)$ is already of order $\alpha_S{}^2$. To extract $\Lambda_{\overline{MS}}$ we need to calculate E, V_1, and V_2 to order $\alpha_S{}^3$.

Case (4): $V_1^N=-V_2^N$ so that $V_1^N=-V_2^N=-\frac{1}{2}E^N$. The assumption, made in Ref. 10, that only the color-electric field contributes to the long-range part of the static energy is phenomenologically equivalent to this case:

$$V_L(m,r)=\frac{1}{2}\frac{1}{m^2r}\frac{dE}{dr}(r)+\frac{4}{3}\frac{1}{m^2r^3}\alpha_{\overline{MS}}(\mu)\left[1+\frac{\alpha_S}{\pi}B\right] , \quad (6.4)$$

$$B=\tfrac{1}{2}b_0[\ln(\mu r)+\gamma_E-1]+\tfrac{5}{12}b_0$$
$$-2+\tfrac{3}{2}\{\tfrac{8}{9}-2[\ln(mr)+\gamma_E-1]\} .$$

The results for $\Lambda_{\overline{MS}}$ are shown in Fig. 3 with the other cases.

The nonperturbative contributions are what cause the fluctuations in Fig. 1. Positive nonperturbative contributions cause the value of $\Lambda_{\overline{MS}}$ extracted from the data to be larger than the proper value, negative nonperturbative contributions shift it down. We naively expect the nonperturbative contributions to come with different signs in different physical processes so that the mean of Fig. 1 should correspond to the physical Λ parameter of QCD. The size of the shifts in Fig. 3 depends on how we choose to include long-range contributions.

Figure 3 shows that the electric confinement model is disfavored. Although we have not extracted $\Lambda_{\overline{MS}}$ for the $V_1^N=0$ case, this model gives values of $\Lambda_{\overline{MS}}$ below those of the electric confinement model, and is probably ruled out. For the spin-orbit force in $(c\bar{c})$ the data indicate that the net nonperturbative contribution is negative; but the size of the shifts in $(b\bar{b})$ is comparable to the experimental errors. Better data will be able to distinguish the model of short-range spin forces from the model of scalar long-range forces and other models.

VII. REVIEW OF OTHER MODELS OF SPIN SPLITTINGS

All models of heavy quarkonium agree on the spin-averaged energy-level spectrum even though many different quarkonium potentials are used. Consequently the wave functions and masses that are contained in these models are not identical but are all very similar. Since the factors needed in the spin splittings are relatively insensitive to the wave function, variations here should not give rise to large differences in the models. To compare the various theoretical calculations we look at what they use for V_L and V_T. At short distances the forms of V_L and V_T are predicted by QCD from perturbation theory:

$$V_L=2\frac{\alpha_S}{m^2}\frac{1}{r^3}[1+O(\alpha_S)] ,$$
$$V_T=\frac{4}{3}\frac{\alpha_S}{m^2}\frac{1}{r^3}[1+O(\alpha_S)] . \quad (7.1)$$

The expansion parameter becomes large at long distances so Eqs. (7.1) break down there. All models based on QCD must agree with Eqs. (7.1) at short distances but the various models differ in the numerical values used for α_S. The models also differ in the long-distance behaviors of V_L and V_T, since this cannot be determined by perturbation theory.

The predictions of the various models are sensitive to how the parameters such as α_S, etc., are chosen (usually from charmonium data). To minimize the sensitivity to the parameters and to elucidate the importance of the long-distance terms we examine the quantity R, the ratio of the fine-structure splittings:

$$R=\frac{M_2-M_1}{M_1-M_0}=2-\frac{36}{10\dfrac{\langle V_L\rangle}{\langle V_T\rangle}+15} . \quad (7.2)$$

Using just the short-distance terms from Eqs. (7.1)

$$R=\tfrac{4}{5}+O(\alpha_S) .$$

Since α_S, m, and $\langle 1/r^3\rangle$ essentially cancel out in this ratio, it should be useful for comparing the models if the short-distance contribution is significant. The order-α_S corrections to this ratio are small.

Figure 4 shows the consistency between the long-range behavior of the V's and the value of R. The Buchmüller (BG) (Refs. 11 and 12), MB (Ref. 14), and GRR (Ref. 16) models have ratios smaller than the tree level since they have a long-distance term in V_L that is negative, making V_L smaller [see Eq. (7.2)]. The EF (Ref. 10) and Gottfried (G) (Ref. 38) models have a ratio larger than the tree level since they have a positive long-distance term in V_L. The G model has a larger ratio than the EF model because G takes the EF model and reduces the size of α_S in it—making the long-distance term more important.

MR have positive long-distance terms in both V_L and V_T. They obtain a very small ratio so the contribution of the long-distance part of V_T must be quite substantial.

In the models of MR and MB some relativistic corrections are taken into account in the zero-order wave functions used for computing Eqs. (5.1). As noted previously, the fine-structure energy splittings should not be sensitive to such corrections. We should expect, and Fig. 4 seems to confirm, that the dominant difference in the tabulated models should be their choices for V_L and V_T. The MB and MR models have $(b\bar{b})$ ratios that are very small—only slightly bigger than the ratios they predict for charmonium. Both of these models take the size of the short-distance contribution from the spin-independent potential and then weaken it with exponential damping factors. Because $(b\bar{b})$ probes shorter distances than charmonium, the ratios are slightly larger and hence closer to the tree-level predictions but not as large as one would expect if the tree-level terms were undamped.

The GRR model includes the order α_S corrections to the tree-level terms to get a better expression for V_L and V_T at short distances. These corrections also lower the value for R. However, GRR choose their short-distance parameters consistent with the rather small value of $\Lambda^{(5)}_{\overline{\rm MS}}=108$ MeV. As in the G model, by making the coupling constant small the importance of the long-distance terms is increased (and the effect of the one-loop correction is decreased). Thus their values of R are very similar to those of BG.

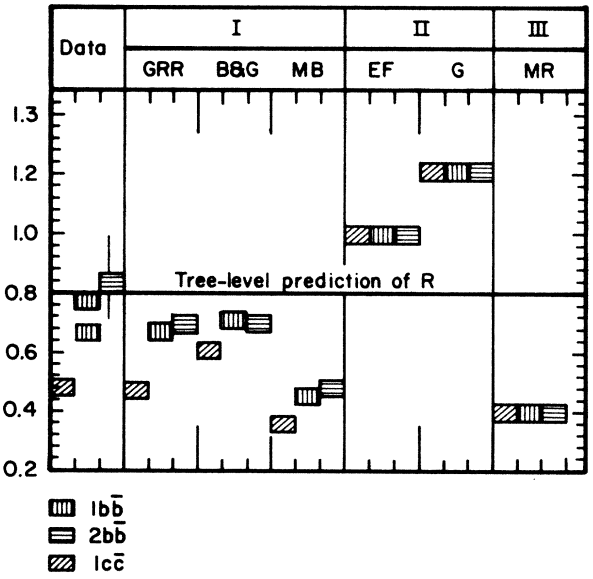

FIG. 4. Comparing different theoretical predictions for R, the ratio of the energy level splittings, with the data: $R=(M_2-M_1)/(M_1-M_0)$. Two values of R for $(b\bar{b})$ $1P$ state are included. The larger value is that quoted in the text. The lower value is that quoted in the *Note added.* Group I are those models that have a negative long-range term in the spin-orbit potential and no long-range term in the tensor potential; GRR (Ref. 16), BG (Refs. 11 and 12), and MB (Ref. 14). Group II are those models that have a positive long-range term in the spin-orbit potential and no long-range term in the tensor potential; EF (Ref. 10) and G (Ref. 38). Group III is the model with positive long-range terms in the spin-orbit and tensor potentials; MR (Ref. 13). Since the results for the $2P$ states have not been independently verified the experimental uncertainty of R for the $2P$ states has been chosen to match the uncertainty for the $1P$ states which comes from Table I.

From this comparison of many dissimilar models we can draw some conclusions.

(1) The perturbative QCD piece is the largest part of the V_L's.

(2) The importance of the long-range part depends on the magnitude of the parameters, α_S, etc. The coefficient of the long-range part of V_L is usually chosen to have the same magnitude as that of the spin-averaged potential. The size of the short-distance contribution is determined by the choice of α_S. This is usually taken to be the same as the spin-average force or put in by hand. The smaller the value of α_S that one puts in, the larger the effect of the nonperturbative, long-range part.

(3) Most models treat the spin-dependent forces the same way as they treat the spin-averaged forces. For both forces, they start with the perturbation QCD short-distance expression (usually the tree level) and then add an *ad hoc*, long-range, nonperturbative term (the assumption is usually flavor independent); next they fit parameters with charmonium data and then try to predict the $(b\bar{b})$ values.

(4) The vector long-range case is probably ruled out.

VIII. PREDICTIONS

Not all of the spin splittings observed in $(c\bar{c})$ have been observed in the $(b\bar{b})$ system. Table XI contains the predictions for the hyperfine splittings of the S states of $(b\bar{b})$. It also contains predictions for the fine-structure states since the experimental errors for the fine-structure splittings are still quite large.

The value of $\Lambda_{\overline{\rm MS}}$ used in the perturbative expression for the V's has been taken to be the average obtained from Fig. 1, namely, $\Lambda_{\overline{\rm MS}}=300\pm60$ MeV. (See *Note added.*) The extracted value of $\Lambda_{\overline{\rm MS}}$ may be used with the RBGT potential to give accurate predictions of the $(b\bar{b})$ splittings. Overall shifts of the wave-function factors will cancel out in the predictions for the fine and hyperfine splittings of $(b\bar{b})$. The only uncertainty in the predictions is taken to be due to the uncertainty in $\Lambda_{\overline{\rm MS}}$.

Besides the unknown splittings of $(b\bar{b})$ we make predictions for the spin splittings of the t-quarkonium energy levels in Tables XII and XIII. For this system the relativistic and nonperturbative corrections should be negligible. The largest uncertainty in our predictions for t quarkonium will be in the wave-function-dependent factor. No energy levels in the t-quarkonium system have yet been measured so we cannot yet test the accuracy of the phenomenological potential here. However, since $(t\bar{t})$ will probe short distances (Table X) the form of the potential is known from perturbation theory. The BGT potential incorporates these short-distance predictions into its definition; unfortunately it uses a value of $\Lambda_{\overline{\rm MS}}$ that is too large, i.e., $\Lambda_{\overline{\rm MS}}=0.50$ GeV. This will have little effect on the value of R in the fine structure since here the nonperturbative factor cancels out, but it will effect the size of the energy-level splittings.

TABLE XII. The hyperfine splittings using the one-loop perturbative expressions. We take $\Lambda_{\overline{\rm MS}}$ to be 300±60 MeV, for $N_F=3$. The fourth column gives the one-loop correction in the BLM prescription. (a) The BGT potential, $N_F=3$. (b) The patched potential, $N_F=4$. (c) The patched potential $N_F=5$.

State	BLM μ (GeV)	BLM ΔE (MeV)	Corr. (percent)	Grunberg μ (GeV)	Grunberg ΔE (MeV)
		(a)			
$Q\bar{Q}$ $1S$ $M_Q=30.0$ GeV	7.10	29.5±0.6	−35.0	29.3	32.9±1
$Q\bar{Q}$ $1S$ $M_Q=40.0$ GeV	8.90	30.3±0.6	−35.0	39.5	33.8±1
$Q\bar{Q}$ $1S$ $M_Q=50.0$ GeV	10.6	31.3±0.6	−34.0	49.7	34.8±1
$Q\bar{Q}$ $1S$ $M_Q=60.0$ GeV	12.3	32.3±0.6	−34.0	60.0	35.9±1
		(b)			
$Q\bar{Q}$ $1S$ $M_Q=30.0$ GeV	6.28	16.7±0.2	−42.0	33.9	19.8±0.7
$Q\bar{Q}$ $1S$ $M_Q=40.0$ GeV	7.98	18.0±0.3	−40.0	45.7	21.0±0.7
$Q\bar{Q}$ $1S$ $M_Q=50.0$ GeV	9.62	19.2±0.3	−40.0	57.7	22.4±0.7
$Q\bar{Q}$ $1S$ $M_Q=60.0$ GeV	11.2	20.6±0.3	−39.0	69.8	23.9±0.7
		(c)			
$Q\bar{Q}$ $1S$ $M_Q=30.0$ GeV	6.28	16.8±0.2	−42.0	39.2	20.0±0.7
$Q\bar{Q}$ $1S$ $M_Q=40.0$ GeV	7.98	18.0±0.3	−41.0	53.2	21.3±0.7
$Q\bar{Q}$ $1S$ $M_Q=50.0$ GeV	9.62	19.3±0.3	−40.0	67.4	22.7±0.7
$Q\bar{Q}$ $1S$ $M_Q=60.0$ GeV	11.2	20.7±0.3	−40.0	81.8	24.2±0.7

IX. CONCLUSIONS

In this paper we have shown the importance of the one-loop perturbative QCD contributions to the spin splittings of heavy quarkonium. These terms have been included previously by GRR but we use these terms to qualitatively influence the theoretical nature of our work. We verify to one loop a relation among the spin-independent and spin-orbit forces [Eq. (3.5)]:

$$\frac{d}{dr}[E(r)+V_1(m_1,m_2,r)-V_2(m_1,m_2,r)]=0\ .$$

This relation was proposed by Gromes[12] and follows from Lorentz invariance. The one-loop contributions have determined our formalism for the spin-dependent forces since they force us to modify the EFG formalism by adding [Eq. (3.1)]

$$\left[\left(\frac{\mathbf{S}_1}{m_1{}^2}-\frac{\mathbf{S}_2}{m_2{}^2}\right)\cdot\mathbf{L}+\left(\frac{\mathbf{S}_1-\mathbf{S}_2}{m_1m_2}\right)\cdot\mathbf{L}\right]V_5(m_1,m_2,r)$$

for the unequal-mass case. Lorentz invariance tells us that only one potential V_5 is necessary above and this is verified by the one-loop contributions. For equal- or unequal-mass heavy quarks, the one-loop contributions to the spin forces depend on powers and logarithms of the heavy-quark mass—the spin forces are flavor dependent.

The one-loop terms are crucial to a qualitative analysis of the experimental data. They allow us to relate the data to the fundamental parameter of QCD, the Λ parameter. Each of the eight measured spin splittings yields a value for Λ, the typical value being $\Lambda_{\overline{\rm MS}}=0.30\pm0.06$ GeV (see *Note added*). Fluctuations about a Λ value are caused by effects not included in the perturbative QCD expression, such as long-range effects and relativistic corrections. For $(c\bar{c})$ we see some evidence for these effects in Fig. 1, but for $(b\bar{b})$ all the values for Λ extracted from the data are so far consistent within the experimental errors. Concentrating on the spin-orbit force, we see that some previously proposed models for long-range effects can probably be ruled out (Fig. 3). Better data will certainly provide valuable hints on the size and form of such effects.

A short version of this work has been published in Phys. Rev. Lett. **55**, 916 (1985).

TABLE XIII. The fine-structure splittings using the one-loop perturbative expressions. We take $\Lambda_{\overline{\rm MS}}$ to be 300±60 MeV, for $N_F=3$. The fifth column gives the one-loop correction in the BLM prescription. R is given by $R=(M_2-M_1)/(M_1-M_0)$. (a) The BGT potential, $N_F=3$. (b) The patched potential, $N_F=3$. (c) The patched potential, $N_F=4$.

	BLM				Grunberg		
State	μ (GeV)	R	M_1-M_0 (MeV)	Corr. (percent)	μ (GeV)	R	M_1-M_0 (MeV)
			(a)				
$Q\bar{Q}$ $1P$ spin-orbit	2.57	0.768	8.6±0.2	−33.0	6.76	0.807	9.1±0.3
$Q\bar{Q}$ $1P$ tensor	3.59			−21.0	7.04		
$M_Q=30.0$ GeV							
$Q\bar{Q}$ $2P$ spin-orbit	3.05	0.770	5.2±0.1	−29.0	7.46	0.800	5.3±0.2
$Q\bar{Q}$ $2P$ tensor	4.25			−16.0	7.47		
$M_Q=30.0$ GeV							
$Q\bar{Q}$ $1P$ spin-orbit	3.13	0.776	8.1±0.2	−32.0	8.60	0.809	8.5±0.3
$Q\bar{Q}$ $1P$ tensor	4.37			−21.0	9.13		
$M_Q=40.0$ GeV							
$Q\bar{Q}$ $2P$ spin-orbit	3.69	0.776	4.6±0.1	−28.0	9.40	0.804	4.8±0.1
$Q\bar{Q}$ $2P$ tensor	5.14			−17.0	9.62		
$M_Q=40.0$ GeV							
$Q\bar{Q}$ $1P$ spin-orbit	3.67	0.781	7.7±0.2	−31.0	10.3	0.812	8.2±0.2
$Q\bar{Q}$ $1P$ tensor	5.12			−21.0	11.1		
$M_Q=50.0$ GeV							
$Q\bar{Q}$ $2P$ spin-orbit	4.29	0.781	4.3±0.1	−28.0	11.3	0.806	4.4±0.1
$Q\bar{Q}$ $2P$ tensor	5.99			−17.0	11.8		
$M_Q=50.0$ GeV							
$Q\bar{Q}$ $1P$ spin-orbit	4.18	0.785	7.6±0.2	−31.0	12.0	0.812	8.0±0.2
$Q\bar{Q}$ $1P$ tensor	5.84			−21.0	13.1		
$M_Q=60.0$ MeV							
$Q\bar{Q}$ $2P$ spin-orbit	4.87	0.784	4.0±0.1	−27.0	13.1	0.807	4.2±0.1
$Q\bar{Q}$ $2P$ tensor	6.80			−18.0	13.8		
$M_Q=60.0$ MeV							
			(b)				
$Q\bar{Q}$ $1P$ spin-orbit	2.20	0.764	5.9±0.1	−38.0	6.22	0.812	6.5±0.2
$Q\bar{Q}$ $1P$ tensor	3.08			−25.0	6.69		
$M_Q=30.0$ GeV							
$Q\bar{Q}$ $2P$ spin-orbit	2.67	0.768	4.0±0.1	−32.9	6.92	0.805	4.2±0.1
$Q\bar{Q}$ $2P$ tensor	3.73			−19.0	7.14		
$M_Q=30.0$ GeV							
$Q\bar{Q}$ $1P$ spin-orbit	2.62	0.773	5.0±0.1	−37.0	7.77	0.816	5.4±0.2
$Q\bar{Q}$ $1P$ tensor	3.65			−26.0	8.59		
$M_Q=40.0$ GeV							
$Q\bar{Q}$ $2P$ spin-orbit	3.19	0.775	3.5±0.1	−32.0	8.68	0.808	3.7±0.1
$Q\bar{Q}$ $2P$ tensor	4.45			−21.0	9.17		
$M_Q=40.0$ GeV							
$Q\bar{Q}$ $1P$ spin-orbit	3.02	0.779	4.5±0.1	−37.0	9.29	0.817	4.9±0.1
$Q\bar{Q}$ $1P$ tensor	4.21			−26.0	10.4		
$M_Q=50.0$ GeV							
$Q\bar{Q}$ $2P$ spin-orbit	3.69	0.780	3.2±0.1	−31.0	10.4	0.811	3.4±0.1
$Q\bar{Q}$ $2P$ tensor	5.15			−21.0	11.2		
$M_Q=50.0$ GeV							
$Q\bar{Q}$ $1P$ spin-orbit	3.41	0.784	4.2±0.1	−36.0	10.8	0.819	4.5±0.1
$Q\bar{Q}$ $1P$ tensor	4.76			−26.0	12.3		
$M_Q=60.0$ GeV							
$Q\bar{Q}$ $1P$ spin-orbit	4.17	0.784	3.1±0.1	−31.0	12.1	0.812	3.2±0.1
$Q\bar{Q}$ $1P$ tensor	5.82			−21.0	13.1		
$M_Q=60.0$ GeV							

TABLE XIII. (*Continued*).

State	BLM μ (GeV)	BLM R	BLM M_1-M_0 (MeV)	BLM Corr. (percent)	Grunberg μ (GeV)	Grunberg R	Grunberg M_1-M_0 (MeV)
			(c)				
$Q\bar{Q}$ $1P$ spin-orbit	2.20	0.758	6.0±0.1	−39.0	6.75	0.808	6.6±0.2
$Q\bar{Q}$ $1P$ tensor	3.08			−26.0	7.12		
$M_Q=30.0$ GeV							
$Q\bar{Q}$ $2P$ spin-orbit	2.67	0.762	4.0±0.1	−33.0	7.47	0.801	4.3±0.1
$Q\bar{Q}$ $2P$ tensor	3.73			−20.0	7.52		
$M_Q=30.0$ GeV							
$Q\bar{Q}$ $1P$ spin-orbit	2.62	0.767	5.1±0.1	−38.0	8.48	0.812	5.5±0.2
$Q\bar{Q}$ $1P$ tensor	3.65			−27.0	9.19		
$M_Q=40.0$ GeV							
$Q\bar{Q}$ $2P$ spin-orbit	3.19	0.755	3.5±0.1	−31.0	9.40	0.805	3.7±0.1
$Q\bar{Q}$ $2P$ tensor	4.45			−21.0	9.72		
$M_Q=40.0$ GeV							
$Q\bar{Q}$ $1P$ spin-orbit	3.02	0.773	4.5±0.1	−37.0	10.2	0.813	5.0±0.1
$Q\bar{Q}$ $1P$ tensor	4.21			−27.0	11.2		
$M_Q=50.0$ GeV							
$Q\bar{Q}$ $2P$ spin-orbit	3.69	0.775	3.3±0.1	−32.0	11.3	0.807	3.5±0.1
$Q\bar{Q}$ $2P$ tensor	5.15			−22.0	11.9		
$M_Q=50.0$ GeV							
$Q\bar{Q}$ $1P$ spin-orbit	3.41	0.778	4.3±0.1	−37.0	11.8	0.816	4.7±0.1
$Q\bar{Q}$ $1P$ tensor	4.76			−27.0	13.3		
$M_Q=60.0$ GeV							
$Q\bar{Q}$ $2P$ spin-orbit	4.17	0.778	3.1±0.1	−32.0	13.1	0.809	3.3±0.1
$Q\bar{Q}$ $2P$ tensor	5.82			−22.0	14.0		
$M_Q=60.0$ GeV							

Note added

After the completion of the above work, new data have been published by the Crystal Ball Collaboration [R. Nernst *et al.*, Phys. Rev. Lett. **54**, 2195 (1985)] and by the ARGUS Collaboration [H. Albrecht *et al.*, Phys. Lett. **160B**, 331 (1985)]. From their results, we obtain for the $1P$ splittings in the Υ system:

$$M(1^3P_2)-M(1^3P_1)=21.0\pm1.0 \text{ MeV} ,$$

$$M(1^3P_1)-M(1^3P_0)=30.7\pm1.2 \text{ MeV} ,$$

$$R=0.68\pm0.04 .$$

Using these results and the analysis discussed in the text, we obtain the $\Lambda_{\overline{\text{MS}}}$ for the tensor part of the $1P$ state

$$\Lambda_{\overline{\text{MS}}}=0.41\pm0.04 \text{ GeV} .$$

The $\Lambda_{\overline{\text{MS}}}$ for the spin-orbit (L) part of the $1P$ states depends on the long-range force (with

$$\left\langle \frac{1}{r}\frac{\partial E}{\partial r}\right\rangle =0.36 \text{ GeV}^3$$

and values in Table VII):

case 1: $\Lambda_{\overline{\text{MS}}}=0.34\pm0.02$ GeV ,

case 2: $\Lambda_{\overline{\text{MS}}}=0.40\pm0.02$ GeV ,

case 4: $\Lambda_{\overline{\text{MS}}}=0.02\pm0.01$ GeV .

The results are shown in Fig. 5. It is clear that case 2 (scalar long range) and case 1 (no long range) are compatible with data. The average $\Lambda_{\overline{\text{MS}}}$ becomes

case 1: $\Lambda_{\overline{\text{MS}}}=0.37\pm0.06$ GeV ,

case 2: $\Lambda_{\overline{\text{MS}}}=0.40\pm0.04$ GeV ,

if we use the data from the Υ system only. These values are somewhat larger than the value determined by other means. This allows us to predict the splittings in the excited $2P$ states in the Υ system. Using values in Table VII and

$$\left\langle \frac{1}{r}\frac{\partial E}{\partial r}\right\rangle =0.25 \text{ GeV}^3 ,$$

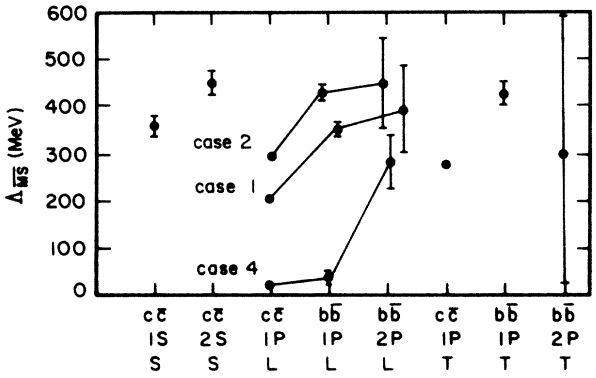

FIG. 5. $\Lambda_{\overline{MS}}$ extracted from the various scenarios discussed in the text. This is the same as Fig. 3 except that the more recent data are used. For details, see the *Note added*. The data are consistent with case 1 (no long range) and case 2 (scalar long range). The $\Lambda_{\overline{MS}} \simeq 0.40$ GeV is obtained.

we predict

$$M(2^3P_2)-M(2^3P_1)=\begin{cases}16.2 \text{ MeV case 1}\\14.9 \text{ MeV case 2}\end{cases},$$

$$M(2^3P_1)-M(2^3P_0)=\begin{cases}21.8 \text{ MeV case 1}\\22.3 \text{ MeV case 2}\end{cases}.$$

The errors are around 1 MeV.

$$R=\begin{cases}0.74 \text{ case 1}\\0.67 \text{ case 2}\end{cases}.$$

ACKNOWLEDGMENTS

We thank K. Gottfried, E. Eichten, G. P. Lepage, S. R. Radford, J. L. Rosner, J. Sapirstein, and T. M. Yan for useful discussions. Y.J.N. also thanks the Theory Group at SLAC for hospitality and A. Halprin for the hospitality extended to him at the Lewes Center for Physics where part of this work was done. Y.J.N. was supported in part by the DOE and the Alfred P. Sloan Foundation. J.P. and S.-H.H.T. were supported by the National Science Foundation.

APPENDIX A

In this appendix we explain briefly the BLM prescription[36] and the Grunberg prescription[35] used in the text. The difference between the various prescriptions is at higher orders in α_S, which have not been calculated. Hence each prescription attempts to estimate the contribution from higher orders and include as much of these effects as possible into the formula that has been calculated.

Let us consider a physical quantity P for which perturbative QCD gives the following form:

$$P=C_0\left[\frac{\alpha_S(\mu)}{4\pi}\right]^N\left[1+C_1(\mu)\frac{\alpha_S(\mu)}{4\pi}+C_2(\mu)\frac{\alpha_S{}^2(\mu)}{(4\pi)^2}+\cdots\right], \quad \text{(A1)}$$

where N is a power depending on the process considered. The coefficients $C_i(\mu)$ depend on (a) the renormalization scheme employed to calculate P, and (b) the choice of mass scale μ. In any finite-order analysis, different choices of scheme and scale give different results for P. Here we will not discuss the different renormalization schemes.[39] Let us just say that we have already chosen a particular renormalization scheme, say, the $\overline{MS}$ (modified minimal-subtraction)[8] scheme. We now turn to the scale-fixing ambiguity and explain the BLM and Grunberg prescriptions.

Brodsky *et al.* argue that, as in QED, the only function of light-fermion insertions in the gauge-particle propagator is to renormalize the couplings, and hence all such terms should be completely absorbed into α_S. Furthermore, since α_S is essentially a function of $b_0=11-\frac{2}{3}N_F$ (N_F is the number of light-quark species) one can use the light-quark loops as a probe to absorb the necessary amount of gluonic corrections. In essence, the BLM prescription requires one to identify the N_F terms from which one forms the b_0 combination, and then the mass scale for the process under consideration is fixed by demanding the coefficient of b_0 to be zero. Examples relevant to the processes we consider in this paper can be found in Ref. 17.

On the other hand, the Grunberg prescription involves choosing the scale μ for the process under consideration in such a way that the lowest-order formula for that process is exact, i.e., so that the one-loop coefficient vanishes. Let us consider a certain physical quantity P for which the lowest-order formula yields

$$P=C_0[\rho(Q^2)_G]^N, \quad \text{(A2)}$$

where we have denoted $\alpha_S/4\pi$ by ρ and the subscript G refers to the Grunberg prescription for which the formula is exact. For large Q^2/Λ^2, $\rho(Q^2)_G$ has the asymptotic expansion[35]

$$\rho(Q^2)_G=\frac{1}{b_0}\left[\frac{1}{\ln\frac{Q^2}{\Lambda^2}}-\frac{b_1\ln\ln\frac{Q^2}{\Lambda^2}}{\left[b_0\ln\frac{Q^2}{\Lambda^2}\right]^2}\right]+\cdots. \quad \text{(A3)}$$

If, in a particular scheme, say, the $\overline{MS}$ scheme, the quantity P is given to one-loop corrections by

$$P=C_0[\rho_{\overline{MS}}(Q^2)]^N[1+C_1(Q^2)\rho_{\overline{MS}}(Q^2)], \quad \text{(A4)}$$

we then can identify

$$\begin{aligned}\rho(Q^2)_G&=\rho_{\overline{MS}}(Q^2)\left[1+\frac{C_1(Q^2)}{N}\rho_{\overline{MS}}(Q^2)\right]\\&=\rho_{\overline{MS}}(\mu^2)\left[1+\left[\frac{C_1}{N}-b_0\ln\frac{Q^2}{\mu^2}\right]\rho_{\overline{MS}}(\mu^2)+\cdots\right],\end{aligned} \quad \text{(A5)}$$

where, for the second step, we have expanded $\rho_{\overline{MS}}(Q^2)$ in terms of $\rho_{\overline{MS}}(\mu^2)$. The Grunberg prescription requires one to choose the mass scale μ^2 such that

$$\frac{C_1}{N}-b_0\ln\frac{Q^2}{\mu^2}=0\ .$$

Up to the second order this choice gives

$$P=C_0[\rho_{\overline{\rm MS}}(\mu)]^N\ . \tag{A6}$$

One can solve (A5) to yield $\Lambda_{\overline{\rm MS}}$ in terms of Λ:

$$b_0\ln\frac{\Lambda^2}{\Lambda^2_{\overline{\rm MS}}}=\frac{C_1}{N}\ . \tag{A7}$$

With P given by experimental data, one can use (A2) and (A3) to extract Λ and then Eqs. (A4) and (A7) to find $\Lambda_{\overline{\rm MS}}$. Also see Appendix C. Finally we note that the Grunberg prescription is very similar in numerical results to the one proposed by Stevenson.[35]

APPENDIX B

In this appendix we briefly describe the patched potential which we have used in the text. The patched potential is intended to be more accurate than other phenomenological potentials at short distances. All phenomenological potentials which successfully reproduce the $(c\bar{c})$ and $(b\bar{b})$ spin-independent spectra agree in the range $0.1\le r\le 1$ fm. Thus the form of the quark-antiquark potential is essentially known in this region. The spin-dependent energy-level splittings probe shorter-distance scales than the spin-independent splittings so, for the calculations in the text, we want a potential that is accurate at distance scales shorter than those usually probed. At short-distance scales perturbative QCD is valid and predicts the potential. Thus, to get an accurate potential, we patch the QCD prediction at short distances, onto the known form of the potential at long distances.

The problem with QCD predictions is that the fundamental parameter of QCD, the Λ parameter, is not accurately known. Reference 6 joined together the perturbative QCD prediction with the Richardson (R) potential[4] using three light-quark flavors and a value of $\Lambda_{\overline{\rm MS}}=500$ MeV. Recent experimental evidence, e.g., the hadronic decay rate for Υ, suggests that this parameter may be as small as 150 MeV. In the text the value of 300 ± 60 MeV emerges from the spin-splitting data. We patch together a new potential using the value of $\Lambda_{\overline{\rm MS}}$ from the text.

To construct the patched potential we use the perturbative QCD prediction

$$\bar{E}(r)=-\frac{1}{r}C_F\alpha_{\overline{\rm MS}}(\mu)\left[1+\frac{\alpha_S}{\pi}\left[\frac{b_0}{2}[\ln(\mu r)+\gamma_E]+\tfrac{5}{12}b_0-\tfrac{2}{3}C_A\right]\right], \tag{B1}$$

where we have neglected relativistic corrections. The full two-loop correction term is not known so we have not included it. To get the size of the coupling constant for Eq. (B1), we numerically invert

$$\rho=\frac{\alpha_{\overline{\rm MS}}(\mu)}{4\pi}\ ,$$

$$\ln\frac{\mu^2}{\Lambda_{\overline{\rm MS}}{}^2}=\frac{1}{b_0\rho}+\frac{b_1}{b_0{}^2}\ln\left[\frac{b_0\rho}{1+\frac{b_1}{b_0}\rho}\right],$$

which is the integral of the perturbative β function [see Eq. (5.3)]. The b_k's are flavor-dependent coefficients:

$$b_0=\tfrac{11}{3}C_A-\tfrac{4}{3}T_FN_f\ ,$$

$$b_1=\tfrac{34}{3}(C_A)^2-\tfrac{20}{3}C_AT_FN_f-4C_FT_FN_f\ .$$

For three flavors ($N_f=3$), $b_0=9$ and $b_1=64$.

We want the patched potential to be accurate over a large energy range so we must take into account the flavor thresholds associated with charm and bottom. In the standard $\overline{\rm MS}$ scheme, N_F is specified to be the number of quark flavors with mass $\le\mu$. New flavor thresholds are treated as step functions in the b_k's at $\mu=$quark masses, so that $\alpha_S(\mu)$ is continuous but its derivative is discontinuous at those values.[34] The different $\Lambda^{(N_F)}_{\overline{\rm MS}}$'s of these effective theories are

$$\Lambda^{(3)}_{\overline{\rm MS}}=300\ \text{MeV}\ ,$$

$$\Lambda^{(4)}_{\overline{\rm MS}}=245\ \text{MeV}\ ,$$

$$\Lambda^{(5)}_{\overline{\rm MS}}=165\ \text{MeV}\ .$$

We choose to specify μ in Eq. (B1) using the BLM prescription.[36] Under this prescription, $\mu_{\rm BLM}$ and $\bar{E}(r)$ are independent of N_F and all of the flavor dependence is in the β function:

$$\mu_{\rm BLM}=\frac{1}{r}\exp[-(\gamma_E+\tfrac{5}{6})]\ ,$$

$$\bar{E}(r)=-\frac{1}{r}C_F\alpha_{\overline{\rm MS}}(\mu_{\rm BLM})\left[1-\frac{\alpha_S}{\pi}(\tfrac{2}{3}C_A)\right]. \tag{B2}$$

Since the coupling constant is continuous at the flavor thresholds so is $\bar{E}(r)$.

At long distances we choose to patch the perturbative expression onto the RBGT potential. The point where we cross over from one region to the other is uniquely defined by requiring the potential and its first derivative to be continuous at the patching point. The point thus determined is at 0.14 fm.

The patched potential predicts almost the identical spin-independent $(c\bar{c})$ and $(b\bar{b})$ spectrum as the RBGT potential. The only difference is that the $(b\bar{b})$ $1S$ state is raised by 20 MeV relative to the other $(b\bar{b})$ states. This is to be expected since the new potential, with a smaller coupling constant, is less steep at short distances than the BGT potential because the coupling constant is now smaller there. The accuracy of the predictions of the RBGT potential is of order 10–20 MeV, roughly the expected size of spin-independent relativistic corrections. The shift of the $1S$ state is thus a small change and will be ignored.

The predictions of the patched potential for the spin-splitting matrix elements are given in Table VII.

APPENDIX C

In the text the $(Q\bar{Q})$ spin splitting data are analyzed in many ways. $\Lambda_{\overline{\rm MS}}$ is extracted from the data for various forms of the long-range spin-orbit force and two different prescriptions. Below we present the equations for extracting $\Lambda_{\overline{\rm MS}}$ using the perturbative QCD expressions with no additional long-range contribution. For simplicity, the Grunberg prescription is used. The method used for including long-range contributions is outlined in the text.

Equations (5.1) and (5.2) relate the experimental data for the spin splittings to the theoretical expressions for the potentials. Inverting Eqs. (5.1) we obtain

$$\langle nP \mid V_L \mid nP\rangle = \tfrac{1}{12}[5M(n^3P_2)-3M(n^3P_1)-2M(n^3P_0)] , \tag{C1}$$

$$\langle nP \mid V_T \mid nP\rangle = -\tfrac{5}{18}[M(n^3P_2)-3M(n^3P_1) +2M(n^3P_0)] , \tag{C2}$$

$$\langle nS \mid V_S \mid nS\rangle = M(n^3S_1)-M(n^1S_0) . \tag{C3}$$

Substituting in the perturbative expressions for V_L, V_S, and V_T one can solve for α_S. We evaluate these expressions for QCD with three light flavors. From the spin-orbit force

$$\alpha_{\overline{\rm MS}}(\mu_L)=\frac{m^2}{2\left\langle\frac{1}{r^3}\right\rangle}\langle nP \mid V_L \mid nP\rangle ,$$

$$\mu_L = m_Q \exp\left[-0.5684-\frac{5}{9}\frac{\left\langle\frac{\ln(mr)-0.4228}{r^3}\right\rangle}{\left\langle\frac{1}{r^3}\right\rangle}\right] . \tag{C4}$$

From the tensor force

$$\alpha_{\overline{\rm MS}}(\mu_T)=\frac{m^2}{\frac{4}{3}\left\langle\frac{1}{r^3}\right\rangle}\langle nP \mid V_T \mid nP\rangle ,$$

$$\mu_T = m_Q \exp\left[-1.0185-\frac{1}{3}\frac{\left\langle\frac{\ln(mr)-0.7561}{r^3}\right\rangle}{\left\langle\frac{1}{r^3}\right\rangle}\right] . \tag{C5}$$

From the spin-spin force

$$\alpha_{\overline{\rm MS}}(\mu_S)=\frac{\langle nS \mid V_S \mid nS\rangle}{\frac{8}{9}\frac{1}{m^2}\mid R_n(0)\mid^2} ,$$

$$\mu_S = m_Q \exp\left[-0.1252-\frac{1}{12}\frac{\left\langle\frac{1}{2\pi}\nabla^2\left[\frac{\ln(mr)+\gamma_E}{r}\right]\right\rangle}{\mid R_n(0)\mid^2}\right] . \tag{C6}$$

The wave-function-dependent factors are given in Table VII. They have been calculated for different quarkonium masses using the RBGT potential and the patched potential (see Appendix B). Using the experimental data and the wave-function factors one gets a numerical value for $\alpha_{\overline{\rm MS}}(\mu)$ and μ. This is then inserted in Eq. (5.3). For QCD with three light flavors

$$\rho=\frac{\alpha_{\overline{\rm MS}}(\mu)}{4\pi} ,$$

$$\Lambda_{\overline{\rm MS}}=\mu\exp\left\{\left[\left[-\frac{1}{2}\right]\left[\frac{1}{9\rho}+\frac{64}{81}\ln\left[\frac{9\rho}{1+\frac{64}{9}\rho}\right]\right]\right]\right\} \tag{C7}$$

$$+\text{higher-order corrections} .$$

---

*Present address: Department of Physics, Purdue University, West Lafayette, IN 47907.

[1]T. Appelquist and D. H. Politzer, Phys. Rev. Lett. **34**, 43 (1975); E. Eichten, K. Gottfried, T. Kinoshita, J. Kogut, K. D. Lane, and T. M. Yan, *ibid.* **34**, 369 (1975). For a representative list see, e.g., K. Gottfried, in *Proceedings of the Conference on High Energy Physics, Brighton, 1983,* edited by J. Guy and C. Costain (Rutherford Appleton Laboratory, Chilton, Didcot, England, 1983). For reviews, see, e.g., K. Berkelman, Phys. Rep. **98C**, 145 (1983); J. Lee Franzini and P. Franzini, Ann. Rev. Nucl. Part. Sci. **33**, 1 (1983); M. E. Peskin, in *Proceedings of the 1983 SLAC Summer Institute on Particle Physics,* edited by P. McDonough (SLAC, Stanford, California, 1983), p. 151; E. Eichten, in *Proceedings of the 1983 SLAC Summer Institute on Particle Physics,* p. 497.

[2]A. Khare, Phys. Rev. D **18**, 4282 (1978); F. Wilczek and A. Zee, Phys. Rev. Lett. **40**, 83 (1978); J. M. Richard and D. P. Sidhu, Phys. Lett. **83B**, 362 (1979); C. A. de Carvalho, Phys. Rev. D **19**, 2502 (1979); N. Barik and S. N. Jena, Phys. Lett. **97B**, 265 (1980); A. B. Henriques, Z. Phys. C **11**, 31 (1981); A. Martin and J. M. Richard, Phys. Lett. **115B**, 323 (1982); J. R. Hiller, Ann. Phys. (N.Y.) **144**, 58 (1982); P. Falkensteiner, D. Flamm, and F. Schoberl, Phys. Lett. **131B**, 450 (1983); A. D. Steiger, *ibid.* **129B**, 335 (1983); J. Morishita, M. Oka, M. Kaburagi, H. Munakata, and T. Kitazoe, Z. Phys. C **19**, 167 (1983); A. T. Aerts and L. Heller, Phys. Rev. D **29**, 513 (1984); D. Sen, Nucl. Phys. **B254**, 678 (1985); J. Rosner, Chicago Report No. EFI 84/33-CHICAGO, 1984 (unpublished); M. Campostrini, Nucl. Phys. **B256**, 717 (1985); M. Klein and O. Streit, Phys. Lett. **146B**, 357 (1984); P. de Forcrand and J. Stack, Phys. Rev. Lett. **55**, 1254 (1985).

[3]E. Eichten, K. Gottfried, T. Kinoshita, K. D. Lane, and T. M. Yan, Phys. Rev. D **17**, 3090 (1978); **21**, 203 (1980); Y. P. Kuang and T. M. Yan, *ibid.* **24**, 2874 (1981).

[4]J. L. Richardson, Phys. Lett. **82B**, 272 (1979).

[5]W. Buchmüller, G. Grunberg, and S.-H. H. Tye, Phys. Rev. Lett. **45**, 103 (1980); **45**, 587(E) (1980).

[6]W. Buchmüller and S.-H. H. Tye, Phys. Rev. D **24**, 132 (1981).

[7]F. L. Feinberg, Phys. Rev. Lett. **39**, 316 (1977); T. Appelquist, M. Dine, and I. Muzinich, Phys. Lett. **69B**, 231 (1977); W. Fishler, Nucl. Phys. **B129**, 157 (1977); A. Billoire, Phys. Lett. **92B**, 343 (1980).

[8]W. A. Bardeen, A. Buras, D. W. Duke, and T. Muta, Phys. Rev. D **18**, 3998 (1978). For a review, see A. J. Buras, Rev. Mod. Phys. **52**, 199 (1980).

[9]E. Eichten, in *Proceedings of the 1983 SLAC Summer Institute on Particle Physics,* Ref. 1; K. Hiekkilä, S. Ono, and N. A. Törnqvist, Phys. Rev. D **29**, 110 (1984).

[10]E. Eichten and F. L. Feinberg, Phys. Rev. Lett. **43**, 1205 (1979); Phys. Rev. D **23**, 2724 (1981).

[11]W. Buchmüller, Phys. Lett. **112B**, 479 (1982); CERN Report No. TH. 3938/84 (unpublished).

[12]D. Gromes, Z. Phys. C **22**, 265 (1984); **26**, 401 (1984).

[13]P. Moxhay and J. L. Rosner, Phys. Rev. D **28**, 1132 (1983).

[14]R. McClary and N. Byers, Phys. Rev. D **28**, 1692 (1983).

[15]W. Buchmüller, Y. J. Ng, and S.-H. H. Tye, Phys. Rev. D **24**, 3003 (1981).

[16]S. N. Gupta, S. F. Radford, and W. W. Repko, Phys. Rev. D **26**, 3305 (1982).

[17]K. Igi and S. Ono, Phys. Rev. D **32**, 232 (1985); H. J. Schnitzer, Phys. Lett. **134B**, 253 (1984); A. B. Henriques, B. H. Kellett, and R. G. Morehouse, *ibid.* **64B**, 85 (1976); P. Hasenfratz, R. R. Horgan, J. Kuti, and J.-M. Richard, *ibid.* **95B**, 299 (1980); J. Baacke, Y. Igarashi, and G. Kasperidus, Z. Phys. C **13**, 131 (1982); R. Barbieri, R. Gatto, and E. Remiddi, Phys. Lett. **106B**, 497 (1981); T. W. Kephart, Y. J. Ng, and H. van Dam, Phys. Rev. D **26**, 3260 (1982).

[18]S. N. Gupta and S. F. Radford, Phys. Rev. D **24**, 2309 (1981); **25**, 2690 (1982). See Ref. 23 for errata. A few other typographical errors have been corrected in our text.

[19]G. 't Hooft, Nucl. Phys. **B61**, 455 (1973); G. 't Hooft and M. Veltman, *ibid.* **B44**, 189 (1972).

[20]W. Celmaster and R. J. Gonsalves, Phys. Rev. D **20**, 1420 (1979).

[21]The terms proportional to $(C_F)^2$ are found in QED. For the spin-independent terms, see B. M. Barder and R. F. O'Connel, J. Math. Phys. **18**, 1818 (1977). For the spin-dependent terms, see T. Fulton and P. C. Martin, Phys. Rev. **95**, 811 (1954).

[22]R. Karplus and A. Klein, Phys. Rev. **87**, 848 (1952).

[23]S. N. Gupta and S. F. Radford, Phys. Rev. D **25**, 3430 (1982). See also M. Klein and O. Streit, Phys. Lett. **146B**, 357 (1984).

[24]B. E. Lautrup, A. Peterman, and E. de Rafael, Phys. Rep. **3**, 193 (1972).

[25]H. Osborn, Phys. Rev. **176**, 1523 (1968); F. E. Close and H. Osborn, Phys. Rev. D **2**, 2127 (1970).

[26]A. Silverman (unpublished).

[27]CUSB Collaboration, C. Klopfenstein *et al.*, Phys. Rev. Lett. **51**, 160 (1983).

[28]CLEO Collaboration, P. Haas *et al.*, Phys. Rev. Lett. **52**, 799 (1984).

[29]Crystal Ball Collaboration, J. Irion *et al.* (unpublished).

[30]Argus Collaboration, J. D. Prentice (private communication).

[31]CUSB Collaboration, C. Klopfenstein *et al.*, Phys. Rev. Lett. **51**, 160 (1983).

[32]Particle Data Group, Rev. Mod. Phys. **56**, S1 (1984).

[33]H. A. Bethe and E. E. Salpeter, *Quantum Mechanics of One- and Two-Electron Atoms* (Plenum/Rosetta, New York, 1977).

[34]W. J. Marciano, Phys. Rev. D **29**, 580 (1984).

[35]G. Grunberg, Phys. Lett. **95B**, 70 (1980); **110B**, 501(E) (1982); Phys. Rev. D **29**, 2315 (1984); See also P. M. Stevenson, *ibid.* **23**, 2916 (1981); M. R. Pennington, *ibid.* **26**, 2048 (1982); W. Celmaster and R. J. Gonsalves, *ibid.* **20**, 1420 (1979).

[36]S. J. Brodsky, G. P. Lepage, and P. B. Mackenzie, Phys. Rev. D **28**, 228 (1983).

[37]R. Barbieri, R. Gatto, and E. Remiddi, Phys. Lett. **61B**, 465 (1976); R. Barbieri, M. Caffo, R. Gatto, and E. Remiddi, Nucl. Phys. **B192**, 61 (1981).

[38]K. Gottfried, in *Proceedings of the Conference on EPS, Brighton, 1983,* edited by J. Guy and C. Costain (Rutherford Appleton Laboratory, Chilton, Didcot, England, 1983), p. 743.

[39]See, e.g., W. Celmaster and D. Sivers, Phys. Rev. D **23**, 227 (1981).